

PRMT3 reverses HIV-1 latency by increasing chromatin accessibility to form a TEAD4-P-TEFb-containing transcriptional hub

Received: 27 June 2024

Accepted: 28 April 2025

Published online: 15 May 2025



Xinyu Wang^{1,11}, Yuhua Xue^{2,11}, Lin Li^{3,11}, Jinwen Song^{4,11}, Lei Jia^{3,11}, Xu Li^{5,11}, Miao Fan¹, Lu Lu^{1,2}, Wen Su¹, Jingwan Han³, Dandan Lin³, Rongdiao Liu^{2,6}, Xiang Gao², Yafei Guo², Zixun Xiang², Chunjing Chen², Linyu Wan⁷, Huihui Chong⁸, Yuxian He⁸, Fusheng Wang⁴, Kaihu Yao¹✉, Qiang Zhou⁹✉ & Dan Yu^{1,10}✉

Latent HIV-1 presents a formidable challenge for viral eradication. HIV-1 transcription and latency reversal require interactions between the viral promoter and host proteins. Here, we perform the dCas9-targeted locus-specific protein analysis and discover the interaction of human arginine methyltransferase 3 (PRMT3) with the HIV-1 promoter. This interaction reverses latency in cell line models and primary cells from latently infected persons by increasing the levels of H4R3Me2a and transcription factor P-TEFb at the viral promoter. PRMT3 is found to promote chromatin accessibility and transcription of HIV-1 and a small subset of host genes in regions harboring the classical recognition motif for another transcription factor TEAD4. This motif attracts TEAD4 and PRMT3 to the viral promoter to synergistically activate transcription. Physical interactions among PRMT3, P-TEFb, and TEAD4 exist, which may help form a transcriptional hub at the viral promoter. Our study reveals the potential of targeting these hub proteins to eradicate latent HIV-1.

A major challenge to the current efforts to cure HIV-1 infection is the persistence of latent viruses¹. Addressing this challenge hinges on unraveling the intricate interplay between the host and viral factors that are key for HIV-1 latency. Current antiretroviral agents effectively prevent actively transcribing viruses from replicating, but have no

activity against the latent viral reservoirs^{2,3}. One of the underlying obstacles is to identify the key chromatin-associated host protein(s) that interact with the 5' long terminal repeats (LTR) containing the viral gene promoter and control viral transcription during latency reactivation^{4–10}. Such interactions are pivotal in determining the fate of

¹Laboratory of Infection and Microbiology, Beijing Pediatric Research Institute, Beijing Children's Hospital, Capital Medical University, Key Laboratory of Major Diseases in Children, Ministry of Education, National Center for Children's Health, Beijing, China. ²State Key Laboratory of Vaccines for Infectious Diseases, Fujian Provincial Key Laboratory of Innovative Drug Target Research, School of Pharmaceutical Sciences, Xiang An Biomedicine Laboratory, Affiliated Xiamen Eye Center, Xiamen University, Xiamen, China. ³State Key Laboratory of Pathogen and Biosecurity, Academy of Military Medical Sciences, Beijing, China.

⁴Senior Department of Infectious Diseases, The Fifth Medical Center of Chinese PLA General Hospital, National Clinical Research Center for Infectious Diseases, Beijing, China. ⁵Department of Dermatology, The First Hospital of Hohhot, Hohhot, China. ⁶Zhejiang Key Laboratory of Intelligent Cancer Biomarker Discovery and Translation, First Affiliated Hospital, Wenzhou Medical University, Wenzhou, China. ⁷The First Affiliated Hospital of University of Science and Technology of China, Division of Life Sciences and Medicine, University of Science and Technology of China, Hefei, China. ⁸NHC Key Laboratory of Systems Biology of Pathogens, Institute of Pathogen Biology and Center for AIDS Research, Chinese Academy of Medical Sciences and Peking Union Medical College, Beijing, China. ⁹School of Biological Sciences, Faculty of Science, The University of Hong Kong, Hong Kong, China. ¹⁰Chinese Institutes for Medical Research, Beijing, China. ¹¹These authors contributed equally: Xinyu Wang, Yuhua Xue, Lin Li, Jinwen Song, Lei Jia, Xu Li. ✉e-mail: yaokaihu@bch.com.cn; qiangz@hku.hk; danyu@ccmu.edu.cn

a virus -- latency versus reactivation -- a balance that must be understood in order for us to achieve the elusive goal of a functional cure for HIV^{11–14}.

Protein arginine methyltransferase 3 (PRMT3), a member of the protein arginine methyltransferase family, functions in epigenetic regulation of gene expression through histone modification¹⁵ and is implicated in a wide array of normal and disease processes ranging from carcinogenesis, hepatic steatosis^{15–29}, to antiviral innate immunity^{17,30}. Given its diverse physiological and pathological functions, significant attention has been directed toward the exploration and development of selective allosteric inhibitors of PRMT3^{31,32}. Despite its well-established functions in many processes of a host cell, the role of PRMT3 in regulating HIV-1 transcriptional reactivation and latency reversal remains largely unclear.

In the current work, we applied a nuclease-deactivated Cas9 (dCas9)-based DNA-protein interaction screen^{8,33,34} to investigate host proteins that potentially interact with the HIV-1 5' LTR. This viral DNA interactome screen has identified PRMT3 as a top candidate. Subsequent functional characterization demonstrates that PRMT3 interacts with the LTR to regulate Tat-dependent reactivation of HIV-1 transcription by regulating the H4R3Me2a level and increasing chromatin accessibility at the viral LTR. This increased accessibility creates a transcriptional hub wherein PRMT3 forms a complex with transcription factors TEAD4 and P-TEFb. The interaction between PRMT3 and TEAD4, and their co-regulation of HIV-1 transcription through binding to the TEAD4-recognition motifs within the LTR, reveal a regulatory pathway whereby host protein and viral DNA interact to control HIV-1 gene expression. Thus, in addition to depicting a previously unrecognized role of PRMT3 as a key host factor that controls viral transcription and latency reversal, our findings establish a basis for the future development of targeted therapeutics for combating HIV-1 infection and latency.

Results

dCas9-targeted HIV-1 LTR-interactome analysis identified PRMT3 as a LTR-binding factor

Seeking host factors that specifically associate with the HIV-1 LTR, we conducted an LTR-interacted proteome analysis based on a refined version of a previously described nuclease-deficient Cas9 (dCas9)-targeted chromatin-based purification strategy (CLASP) (Cas9 locus-associated proteome) (Fig. 1a)^{33,34}. The screen used NH1 cells, which is a modified HeLa cell line that harbors an integrated HIV-1 LTR-driven luciferase reporter gene in the host genome³⁵ (Fig. 1b). To get the most effective sgRNAs that target LTR, we used two methods for screening. We individually inserted the sgRNAs into the Cas9 plasmid, which was then co-transfected with a Tat-expression plasmid into NH1 cells that harbors the LTR-driven luciferase reporter gene. If a sgRNA-Cas9 combination can target and disrupt the LTR sequence, a reduction in luciferase activity is observed. We designed seven sgRNAs targeting different regions of the HIV-1 LTR (Fig. 1b). An sgRNA targeting the yeast Gal4 gene was used as the negative control. Among the designed sgLTRs, the top three sgLTRs (# 5, 6, 7 in pink, Fig. 1b) exhibiting the capacity to attenuate the LTR driven-luciferase expression activated by HIV-1 Tat (Fig. 1c). Then, we performed anti-Flag ChIP-qPCR in cells transfected with the sgLTRs-dCas9-3 × Flag plasmids to further verify the abilities of the sgLTRs to target dCas9-3 × Flag to the LTR, and found that sgLTR-1 and -2 failed to recruit dCas9 to LTR efficiently (Supplementary Fig. 1a, b), sgLTR-5 and -6 displayed the most significant effect, whereas sgLTR-3, -4 and -7 all displayed a similar and partial effect (Supplementary Fig. 1c, d). Thus, sgLTR-5, -6, -7 were selected for subsequent ChIP-qPCR analysis. By utilizing the combination of the three sgRNAs, we found that in comparison to sgGal4, these sgRNAs can guide dCas9 to the LTR as revealed by ChIP-qPCR analysis (Fig. 1d). Next, we performed in vitro transcription reactions to generate these sgRNAs, which were then used for dCas9/sgRNAs

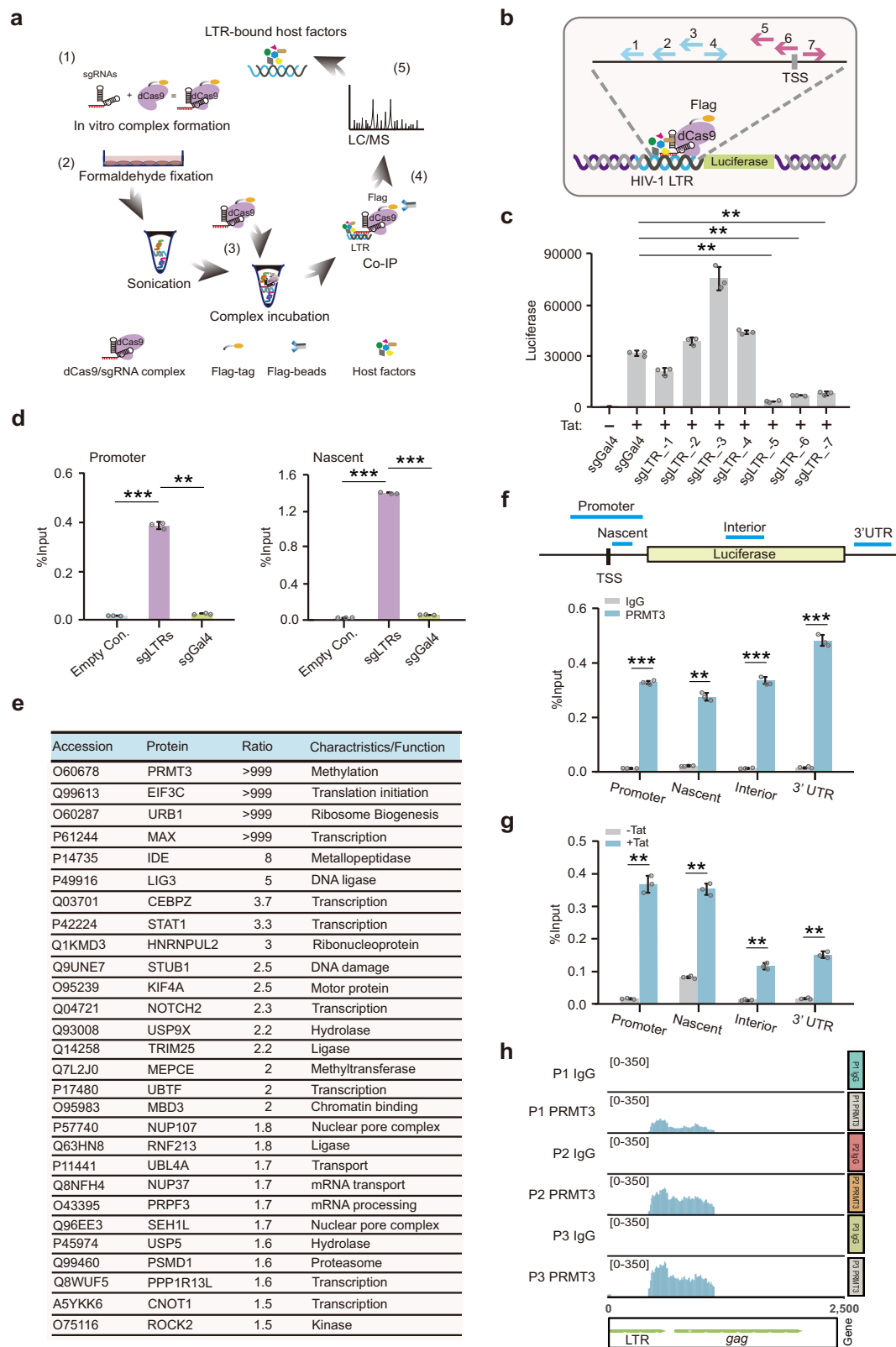
complex formation. This complex was subsequently incubated with sheared chromatin that contained the LTR-bound proteins for dCas9-3 × Flag immunoprecipitation, following with mass spectrometry analysis.

Mass spectrometry detected a total of 28 proteins with at least 1.5-fold enrichment relative to the non-targeting negative control (Fig. 1e and Supplementary Data 1). PRMT3, which has been shown to function in transcriptional regulation and antiviral innate immunity^{15,30,36}, was among the hits with the highest fold enrichment of sgLTR/sgGal4, and was therefore selected for subsequent investigation. We performed ChIP-qPCR analysis to examine the binding of PRMT3 to the LTR. PRMT3 was significantly enriched at LTR-luciferase reporter region (Fig. 1f), which can be further increased in the presence of Tat (Fig. 1g). The binding of PRMT3 at the LTR was also verified in Jurkat 2D10 cells (Supplementary Fig. 2). Notably, we performed Cleavage Under Targets & Tagmentation (CUT&Tag) sequencing by using IgG or PRMT3 antibody in CD4⁺ T cells isolated from HIV-1 infected patient cells, and demonstrated that while IgG displayed undetectable signal at the LTR, PRMT3 showed significant binding signal around LTR (Fig. 1h). Thus, these results demonstrated that PRMT3 is an HIV-1 LTR binding factor, which is further enhanced in the presence of Tat.

PRMT3 enhances Tat-dependent HIV-1 transcription and latency reversal

To examine the potential impact of the HIV-1 LTR-associated PRMT3 on Tat-dependent HIV-1 transcription, we induced PRMT3 knockdown (KD) by shRNAs in NH1 cells. PRMT3 KD did not affect basal HIV-1 transcription but did result in a significant decrease in Tat-dependent viral transcription (Fig. 2a). In contrast, PRMT3 overexpression significantly elevated Tat-dependent but not the Tat-independent HIV-1 transcription (Fig. 2b). The effect of PRMT3 on HIV-1 transcriptional activation was further measured in PRMT3 knockout (KO) cells (Supplementary Fig. 3a, b), which showed no significant defects in cell growth in comparison to the WT cells (Supplementary Fig. 3c). Similar to the KD result above, PRMT3 KO significantly decreased Tat-activated HIV-1 transcription (from 127.5-fold to 25.75-fold), and the plasmid-based re-expression of PRMT3 in the KO cells markedly restored Tat-dependent HIV-1 transcription (from 25.75-fold to 84.12-fold) (Fig. 2c). Together, these results demonstrate that PRMT3 promotes Tat-dependent HIV-1 transcription.

Since JQ1 and phorbol myristate acetate (PMA) are known latency reversal reagents that promote Tat-mediated recruitment of P-TEFb to the HIV-1 LTR to activate transcription^{37–40}, we also monitored PRMT3's effects on HIV-1 transcription upon exposure to JQ1 and PMA. We observed that PRMT3 KO significantly decreased the extent of HIV-1 transcription induced by JQ1 (from 10.35-fold to 4.14-fold) and by PMA (from 20.28-fold to 12.67-fold) (Fig. 2d, e), supporting the view that PRMT3 regulates HIV-1 transcription in a Tat/P-TEFb dependent manner. Furthermore, we also tested the effect of PRMT3 on HIV-1 transcription using a tetracycline inducible shRNA expression system. We found that after doxycycline-induced PRMT3 knockdown using shRNAs targeting two different regions of PRMT3, a significant decrease in Tat-, JQ1-, or PMA-induced HIV-1 transactivation was observed (Supplementary Fig. 4a–c). To investigate whether PRMT3's methyltransferase activity is required for the observed stimulatory effects, we treated NH1 cells with a PRMT3 inhibitor (SGC707)³². The treatment significantly impaired Tat-, JQ1-, and PMA-activated HIV-1 transcription, in a dose-dependent manner (Fig. 2f–h), which showed no obvious inhibitory effect in PRMT3 KO cells (Supplementary Fig. 5a, b). In addition, the catalytic inactive form PRMT3 E338Q was used for further validation of the impact of methyltransferase activity of PRMT3 for HIV-1 transcriptional activation. We found that this E338Q mutant PRMT3 showed significantly decreased ability to support Tat-activation of HIV-1 transcription in comparison to the WT PRMT3 (Supplementary Fig. 5c). These findings establish that PRMT3's



arginine methyltransferase activity contributes to the observed induction of HIV-1 transcription.

To demonstrate that the effect of PRMT3 on HIV-1 transcription contributes to HIV-1 replication, we measured HIV-1 replication in MT4 cells, TZM-bl cells, and in the primary CD4⁺ T cells isolated from virologically suppressed HIV-1-infected patients. MT4 cells were infected with HIV-1 CRF01-AE (GX002: accession: GU564222)⁴¹, which is the

predominantly transmitted HIV-1 strain in China, and treated with DMSO or SGC707. We found that inhibition of PRMT3 by SGC707 significantly decreased the replication of HIV-1 in MT4 cells by measuring the *pol* and *p24* expression levels in the supernatant (Fig. 2i, j). We also constructed PRMT3 gene knockout in the TZM-bl cell line, a HeLa based cell line expressing CD4, CCR5, and CXCR4⁴². WT and PRMT3 KO TZM-bl cells were infected with HIV-1 CRF01-AE.

Fig. 1 | dCas9-targeted HIV-1 LTR-interactome analysis identified PRMT3 as a LTR-binding factor. **a** Schematic of dCas9-targeted proteome analysis workflow. (1) sgRNAs targeting the LTR were complex formation with dCas9-3 × Flag; (2) Crosslinking of proteins bound to the LTR; (3) dCas9-3 × Flag-sgRNA complex was incubated with sheared fragments from NH1 cells that stably expressed LTR-luciferase reporter; (4) Immunoprecipitation was used to capture LTR bound proteins; (5) LTR-interacted proteins were identified by mass spectrometry. **b** Schematic of the position of 7 sgRNAs. **c** Luciferase activity was measured in NH1 cells transfected with a plasmid encoding each sgRNA and control sgRNA (sgGal4), which expresses the Cas9 in the presence of Tat ($p = 0.0016$, $p = 0.0024$, $p = 0.0042$). **d** ChIP-qPCR analyses were conducted to assess the occupancy of 3 × Flag-dCas9 at the Promoter (Left) or Nascent region (Right) of LTR when cells were transfected with control plasmid, a mixture of plasmids containing sgLTRs-5, 6, 7 or the sgGal4 plasmid (Promoter: $p = 0.0009$, $p = 0.0011$, Nascent: $p = 0.000004$,

$p = 0.000003$). **e** Proteins showing over 1.5-fold enrichment relative to the control sample identified from 3 × Flag-dCas9 immunoprecipitation following by mass spectrometry analysis were listed. **f** ChIP-qPCR analyses were conducted to assess the occupancy of PRMT3 at LTR-luciferase region ($p = 0.0001$, $p = 0.0012$, $p = 0.0005$, $p = 0.0008$). The schematic display of the four primers was shown on the top of the panel. **g** ChIP-qPCR analyses were conducted to assess the occupancy of PRMT3 at LTR-luciferase regions in the absence or presence of Tat ($p = 0.0022$, $p = 0.0012$, $p = 0.0045$, $p = 0.0017$). **h** CUT&Tag sequencing was performed in primary CD4⁺ T cells isolated from virologically suppressed HIV-1-infected patient cells that were treated with PMA, by using IgG or PRMT3 antibody. The alignment results of sequencing with the HIV-1 genome in three patients were displayed. Error bars = mean ± SD of three biological replicates. * $p < 0.05$, ** $p < 0.01$, *** $p < 0.001$, two-tailed t test. Source data are provided as a Source Data file.

We showed that knockout of PRMT3 resulted in a decrease in HIV-1 replication by measuring the cellular HIV-1 RNA copies and *gag* expression (Fig. 2k, l). Finally, we measured the effects of PRMT3 knockdown on HIV-1 replication in MT4 cells or primary CD4⁺ T cells isolated from HIV-1 infected patients by targeting PRMT3 using two different PRMT3 siRNAs, and found that knockdown of PRMT3 significantly decrease HIV-1 replication (Supplementary Fig. 6a–e). The impact of PRMT3 on HIV-1 replication was also verified by performing SGC707 treatment, PRMT3 knockdown, or knockout in cells that were infected with another strain, NL4-3 (Supplementary Fig. 7a–e), suggesting that the regulation by PRMT3 on HIV-1 replication is conserved across different HIV-1 subtypes. Together, these data demonstrated that PRMT3 regulates HIV-1 transcription and replication.

Given that HIV-1 transcriptional activation is essential for HIV-1 latency reversal, we anticipated that the inhibition of PRMT3 activity would repress HIV-1 latency reversal. Indeed, experiments involving FACS analysis of a well-known HIV-1 latency model, Jurkat 2D10 cells containing an integrated HIV-1-GFP fusion reporter⁴³, showed that the SGC707-treated group had significantly impeded JQ1- and PMA-mediated latency reversal compared to the vehicle (DMSO) group (Fig. 2m, n and Supplementary Fig. 8a, b). The percentage of GFP⁺ cells indicates the activation effect of HIV-1 transcription (Fig. 2o, p). We then asked whether the inhibition of PRMT3 activity can impair latency reversal of the HIV-1 reservoir in latently infected patients under antiviral treatment. We isolated primary CD4⁺ T cells from 6 HIV-1-infected individuals undergoing suppressive antiretroviral therapy (ART) and then monitored the reactivation of latent HIV-1 transcription (assessed as HIV-1 RNA copies) in cells treated with JQ1 or PMA in the presence or absence of SGC707 (Fig. 2q). The data show that SGC707 significantly inhibited the JQ1- and PMA-induced HIV-1 latency reversal (Fig. 2r, s).

Taken together, the results demonstrate that PRMT3 interacts with the HIV-1 LTR and that its arginine methyltransferase activity promotes Tat-dependent HIV-1 transcription and latency reversal.

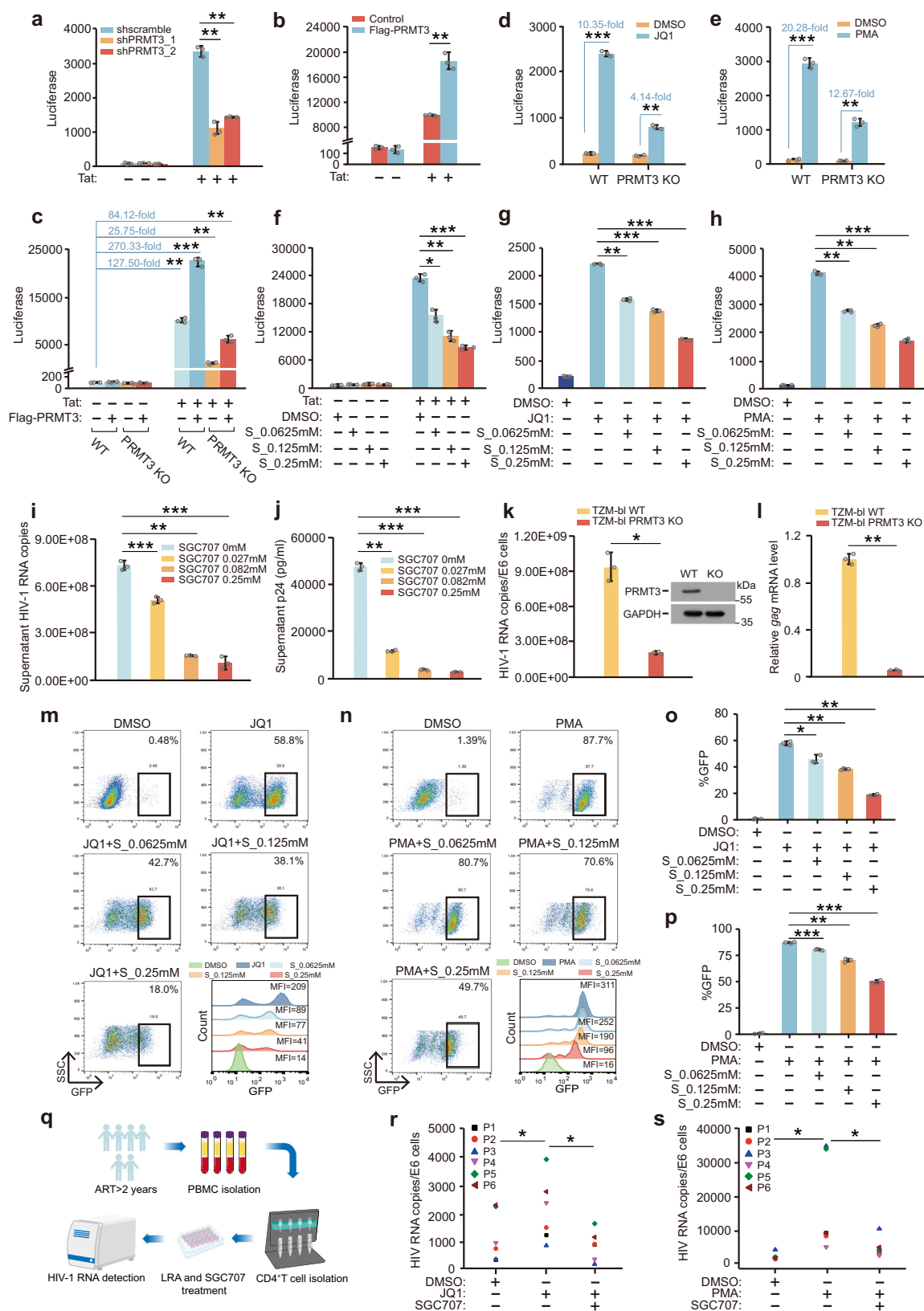
PRMT3 increases H4R3Me2a levels and chromatin accessibility at HIV-1 LTR to promote Tat-dependent recruitment of P-TEFb to the LTR

A previous study reported that PRMT3 activates host gene transcription by enhancing the levels of histone H4 arginine 3 asymmetric dimethylation (H4R3Me2a) at promoter regions¹⁵. In light of these findings and our results showing that the arginine methyltransferase activity of PRMT3 is required for HIV-1 transactivation, we examined whether PRMT3 promotes Tat-activation of HIV-1 transcription by increasing the H4R3Me2a level at the LTR. We examined the global H4R3Me2a levels in wild-type (WT) NH1 and PRMT3 KO cells. Immunoblotting showed a notable reduction in the H4R3Me2a level in the KO cells compared to WT control cells (Fig. 3a). Similarly, reduced H4R3Me2a levels were observed in various cell lines (Jurkat, HeLa, and HEK293T) treated with SGC707 (Fig. 3b).

Next, we investigated the impact of PRMT3 on H4R3Me2a levels specifically at the HIV-1 LTR in WT NH1 and PRMT3 KO cells in the presence of Tat, as well as in NH1 cells expressing Tat and treated with DMSO or SGC707. In both the KO cells and cells upon PRMT3 inhibition, the H4R3Me2a levels were significantly decreased at the LTR (Fig. 3c, d). Having found that PRMT3 deposits H4R3Me2a marks at the LTR, we also performed ATAC-seq in WT and PRMT3 KO NH1 cells that were transfected with a plasmid expressing Tat to examine the effect of PRMT3 on chromatin accessibility at the LTR. Our data showed that the accessibility at the LTR was significantly decreased in PRMT3 KO NH1 cells in comparison to WT cells (Fig. 3e, f). We found that the level of Pol II and Pol II pSer2 decreased at the LTR-luciferase reporter region after PRMT3 KO (Supplementary Fig. 9a, b), which is consistent with the effect of PRMT3 on chromatin accessibility. Together, these data indicate that PRMT3 promotes Tat-activation of HIV-1 transcription by depositing H4R3Me2a marks and enhancing local chromatin accessibility at the LTR.

Given the established mechanism of P-TEFb recruitment to the LTR by Tat for HIV-1 transactivation^{44–46}, we asked whether PRMT3's deposition of H4R3Me2a and change of chromatin accessibility affect the recruitment of P-TEFb. We determined P-TEFb's occupancy at the LTR in WT and PRMT3 KO cells or in DMSO and SGC707 treated FIC2 cells that stably expressed a Flag-tagged CDK9 by conducting anti-Flag-CycT1 or anti-Flag-CDK9 ChIP-qPCR, and discovered a significant reduction in P-TEFb binding at the LTR in PRMT3 KO cells or in SGC707 treated cells (Fig. 3g–i), reinforcing the notion that PRMT3's regulatory effect on HIV-1 transcription involves modulating chromatin accessibility and consequently P-TEFb's recruitment at the LTR.

Next, we investigated whether the impact of PRMT3 on P-TEFb recruitment affected the P-TEFb-mediated Tat-dependent HIV-1 transcription by measuring the luciferase level in HeLa cells that were transfected with an empty control vector or plasmid expressing CycT1 under different conditions. The data showed that a significantly impaired Tat-, JQ1-, or PMA-mediated activation of HIV-1 transcription upon PRMT3 deletion (Fig. 3j–l) or inhibition (Fig. 3m–o) was observed especially when CycT1 was overexpressed. Furthermore, we also determined the dependence on another subunit of P-TEFb, CDK9, for PRMT3-mediated activation of HIV-1 transcription. CDK9 knockdown significantly disrupted PRMT3's stimulatory effect on Tat transactivation (Fig. 3p), further highlighting the requirement of both PRMT3 and P-TEFb for HIV-1 transcriptional activation. To further confirm this point, we co-transfected CycT1 and PRMT3 into NH1 cells to test the effect of co-activation of HIV-1 transcription by PRMT3 and P-TEFb, and observed that the co-expression of CycT1 and PRMT3 resulted in higher transcriptional activation of HIV-1 than the expression of either alone (Fig. 3q). Together, these data suggested that PRMT3 promotes HIV-1 transcription by increasing H4R3Me2a levels and chromatin accessibility at the LTR for enhancement of Tat-dependent recruitment of P-TEFb to the LTR.



PRMT3 affects chromatin accessibility and transcription of a subset of host genes

In addition to PRMT3's stimulatory effect on chromatin accessibility and transcription from HIV-1, we also examined its potential regulation of specific host genes. By performing ATAC-seq in WT and PRMT3 KO NH1 cells, we detected 9392 down-regulated and 6473 up-regulated

regions, including promoter, exon, intron, UTR, and distal intergenic regions in the KO cells (Fig. 4a, Supplementary Fig. 10a-c and Supplementary Data 2). However, PRMT3 does not appear to cause a widespread, global change in chromatin accessibility across the whole genome as evidenced in the analysis from ATAC-seq of WT and PRMT3 KO NH1 cells (Fig. 4b).

Fig. 2 | PRMT3 enhances Tat-dependent HIV-1 transcription and latency reversal. **a–c** Luciferase activities were measured in NH1 cells transfected with shRNA targeting PRMT3 (**a**) ($p = 0.0021$, $p = 0.0024$), Flag-PRMT3 (**b**) ($p = 0.0098$), or in NH1 (WT) and PRMT3 knockout (KO) cells cotransfected with control vector or Tat together with or without Flag-PRMT3 ($p = 0.0012$, $p = 0.0006$, $p = 0.0015$, $p = 0.0053$). **d–h** Luciferase activities were measured in WT and KO cells treated with DMSO, JQ1 (**d**) ($p = 0.0002$, $p = 0.0036$), PMA (**e**) ($p = 0.0009$, $p = 0.0036$), or NH1 cells added with Tat (**f**) ($p = 0.0131$, $p = 0.0050$, $p = 0.0009$), treated with JQ1 (5 μ M) (**g**) ($p = 0.0013$, $p = 0.0004$, $p = 0.00001$) or PMA (200 nM) (**h**) ($p = 0.0022$, $p = 0.0012$, $p = 0.0008$), together with or without SGC707. **i, j** The relative HIV-1 RNA copies (**i**) ($p = 0.0009$, $p = 0.0015$, $p = 0.00003$) and p24 expression (**j**) ($p = 0.0012$, $p = 0.0006$, $p = 0.0006$) in HIV-1 CRF01-AE infected MT4 cells treated

with SGC707 was measured. **k, l** The HIV-1 RNA copies were measured in HIV-1 infected WT or KO TZM-bl cells (**k**) ($p = 0.0122$). The PRMT3 level (right in panel **k**) and relative mRNA level of *gag* was detected (**l**) ($p = 0.0012$). **m, n** Representative flow cytometry analysis of 2D10 cells treated with JQ1 (**m**) or PMA (**n**) with or without SGC707. **o, p** The percentage of GFP⁺ cells indicates the HIV-1 transcription activation (**o**: $p = 0.0184$, $p = 0.0022$, $p = 0.0013$; **p**: $p = 0.0003$, $p = 0.0022$, $p = 0.0006$). **q** Schematic of HIV-1 detection in patients' primary cells. **r, s** HIV-1 RNA copies were detected in CD4⁺ T cells treated with DMSO, JQ1, JQ1 + SGC707 (**r**) ($p = 0.0277$), or PMA, PMA + SGC707 (**s**) ($p = 0.0277$). Error bars = mean \pm SD of three biological replicates except (**r** and **s**) ($n = 6$). * $p < 0.05$, ** $p < 0.01$, *** $p < 0.001$, two-tailed t test. Wilcoxon's matched-pairs signed-rank test was performed in **r** and **s**. Source data are provided as a Source Data file.

To examine the effects of PRMT3-driven chromatin modifications on host gene expression, RNA-Seq analysis was conducted in WT and PRMT3 KO cells, and the results showed that PRMT3 KO resulted in altered expression of 256 genes (119 down-regulated, 137 up-regulated) (Fig. 4c, Supplementary Fig. 10d–f and Supplementary Data 3). Further integrated analysis combining both ATAC-Seq and RNA-Seq showed that only a limited subset of host genes is regulated by PRMT3 through altering chromatin accessibility (Fig. 4d). The signal of chromatin accessibility in WT cells is significantly higher than that in KO cells, which correlates with the gene expression level (Fig. 4e, Up). The signal for each gene was displayed in a row (Fig. 4e, Down). KEGG analysis showed that these PRMT3-regulated genes are predominantly involved in several signaling pathways (Fig. 4f).

A subsequent integrated analysis of the PRMT3 KO cells revealed significant reductions in both chromatin accessibility and expression levels of a few genes, including *PRDM1*, *SLITRK5*, and *TGFB2*, pinpointing specific loci where PRMT3's absence markedly reduced transcriptional activity (Fig. 4g–i). A parallel analysis by qRT-PCR validated that PRMT3 KO resulted in significantly decreased mRNA production from these genes (Fig. 4j–l).

In light of our earlier demonstration that PRMT3 binds to the HIV-1 LTR, we hypothesized that PRMT3 likely associates with the promoter regions of the three genes, *PRDM1*, *SLITRK5*, and *TGFB2*, to deposit H4R3Me2a to activate their transcription. To test this hypothesis, we performed ChIP-qPCR to target multiple promoter regions and detected a significant enrichment of the PRMT3 signal at the tested regions of all three examined loci (Fig. 4m–o). Thus, in addition to showing that PRMT3 binds to the HIV-1 LTR and catalyzes deposition of H4R3Me2a marks that promote Tat-dependent HIV-1 transcription, these results support the notion that PRMT3 also epigenetically regulates the transcription of a subset of host genes that play key roles in certain signal transduction pathways.

PRMT3's association with HIV-1 LTR and host genes requires a classical recognition motif for TEAD4

Next, ATAC-seq footprinting analyses were performed in WT and PRMT3 KO cells to investigate the reason behind the apparently quite narrow specificity of the PRMT3-targeted loci. The analyses using Discriminative Regular Expression Motif Elicitation (DREME) enrichment analyses reveal that PRMT3 impacts accessibility at a specific motif containing a core GGAAT sequence located in a somewhat less conserved but still preferred context containing additional nucleotides (Fig. 5a), a sequence that is also present within the HIV-1 LTR at two distinct locations (Fig. 5b).

To examine the dependence of PRMT3 on this motif for LTR-binding, we constructed two LTR mutants harboring a single $\Delta 13$ bp (–224 – –236bp) or double $\Delta 9 + 7$ bp (–226 – –234bp, +84 – +90 bp) deletions of the core GGAAT sequence plus a few surrounding nucleotides (Fig. 5b). The WT or LTR mutants were fused to a luciferase reporter gene and co-transfected with Tat into HeLa cells. ChIP-qPCR analysis of PRMT3 bound to the WT, $\Delta 13$ bp, or $\Delta 9 + 7$ bp LTR-

luciferase reporter region was performed. We found that the association of PRMT3 with the $\Delta 9 + 7$ bp LTR-luciferase reporter region was significantly decreased (Fig. 5c), while the association of PRMT3 with the $\Delta 13$ bp LTR-luciferase reporter showed no significant change in comparison with the WT (Supplementary Fig. 11), suggesting that PRMT3's activation of HIV-1 transcription is dependent on its association with the motif within LTR.

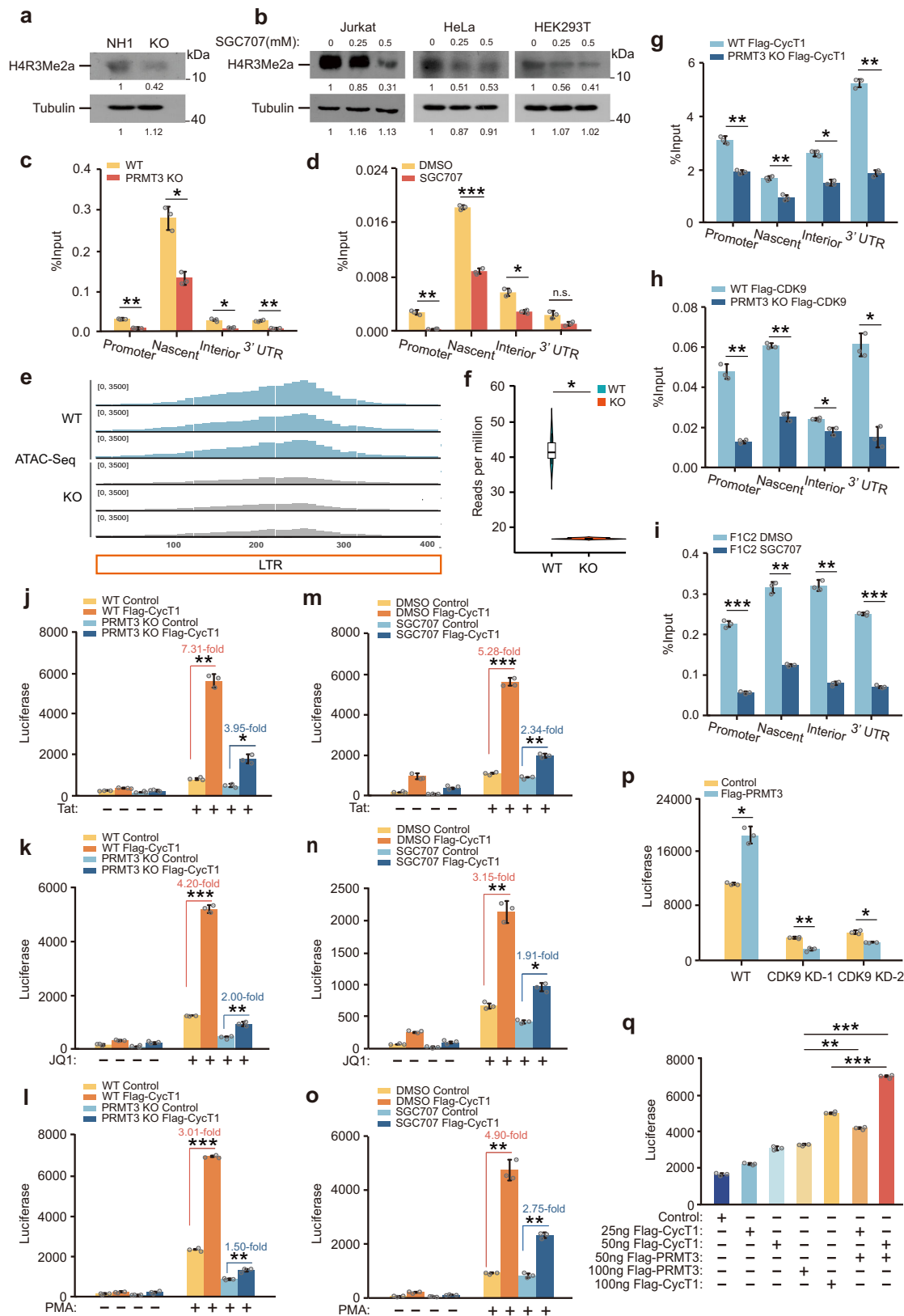
To investigate whether Tat-activated HIV-1 transcription by PRMT3 is dependent on this motif, we cotransfected the WT or mutant LTR constructs with Flag-tagged PRMT3 with or without a Tat-expressing plasmid into HeLa cells. Measurement of luciferase signals showed that Flag-PRMT3 significantly activated Tat-dependent transcription of the WT LTR. In contrast, it failed to activate transcription from the double-deletion mutant $\Delta 9 + 7$ bp LTR, while the $\Delta 13$ bp single deletion resulted in a milder decrease in luciferase signal (Fig. 5d). This result suggests that the activation of HIV-1 transcription by PRMT3 depended on the motif containing the core sequence GGAAT.

Interestingly, this GGAAT sequence is the same core sequence in the known binding motif for sequence-specific transcription factor TEAD4 (Fig. 5e)⁴⁷. Venn diagram analysis of differential expression genes (DEGs) identified in PRMT3 KO cells in the current study compared with those detected in TEAD4 KD cells by Biswarup and colleagues⁴⁸ showed that 30 genes are jointly regulated by both PRMT3 and TEAD4 (Fig. 5f), indicating a possible cooperative transcriptional regulation mechanism facilitated by their interaction at the motif.

PRMT3 co-localizes with TEAD4 at LTR to synergistically activate HIV-1 transcription

To investigate TEAD4's potential contribution to Tat-dependent HIV-1 transcriptional activation, we performed ChIP-qPCR analysis and found that TEAD4 indeed physically associates with the LTR, which is further increased in the presence of Tat (Fig. 5g). Next, we knocked down TEAD4 expression in NH1 cells and found that the KD significantly decreased Tat-dependent but not basal HIV-1 transcription (Fig. 5h). Conversely, NH1 cells transfected with a plasmid over-expressing TEAD4 showed significantly increased Tat-activated HIV-1 transcription (Fig. 5i).

Given this positive effect on Tat-transactivation displayed by TEAD4, we examined whether it is dependent on the GGAAT motif in the LTR. HIV-1 transcriptional activation was measured after co-transfecting HeLa cells with plasmids expressing TEAD4 and the luciferase reporter gene under the control of WT LTR or the mutant LTR lacking both GGAAT motifs. In the presence of Tat, TEAD4 significantly activated Tat-dependent HIV-1 transcription from WT but not the mutant LTR (Fig. 5j). Further ChIP-qPCR analysis of TEAD4's binding to the LTR-luciferase reporter region showed significantly lower TEAD4 binding to the mutant LTR-luciferase reporter region compared to the WT (Fig. 5k). These results demonstrate that TEAD4 activates Tat-dependent HIV-1 transcription by associating with the LTR through the binding motif containing the core GGAAT sequence.



Building upon our aforementioned data illustrating PRMT3's regulation of HIV-1 transcription through modulating chromatin accessibility, we compared TEAD4 enrichment at the LTR between WT and PRMT3 KO cells to determine whether PRMT3 influences TEAD4's recruitment to the LTR. Our ChIP-qPCR analyses showed that in PRMT3 KO cells, there was a significantly decreased TEAD4

occupancy at the LTR-luciferase reporter region (Fig. 5I). Notably, a significant decrease was also observed upon exposure to the PRMT3 inhibitor SGC707 (Fig. 5m). In addition, the binding of TEAD4 in DMSO or SGC707 treated Jurkat 2D10 cells was detected and results showed that TEAD4's association with LTR significantly decreased in SGC707 treated cells (Supplementary Fig. 12).

Fig. 3 | PRMT3 increases H4R3Me2a levels and chromatin accessibility at HIV-1 LTR to promote Tat-dependent recruitment of P-TEFb to the LTR.

a, b H4R3Me2a levels were examined in WT and PRMT3 KO cells (**a**), or in indicated cells treated with DMSO or SGC707 (**b**). Densitometric analyses of immunoblots are shown. **c, d** H4R3Me2a occupancy at LTR-luciferase regions in WT and KO cells (**c**) ($p = 0.0050$, $p = 0.0133$, $p = 0.0102$, $p = 0.0047$), and cells treated with DMSO or SGC707 (**d**) ($p = 0.0064$, $p = 0.0009$, $p = 0.0256$, $p = 0.1042$) were measured. **e, f** ATAC-Seq was performed in WT and KO cells transfected with Tat using three biological replicates (**e**). Normalized depth (Reads per million) was calculated using LTR counts divided by the number of sequences to HIV-1 $\times 1,000,000$. The center line, upper, and lower edges of the boxplot represented the mean, first, and third quartile (**f**). **g–i** WT and KO cells were cotransfected with Tat and Flag-CycT1 (**g**) ($p = 0.0029$, $p = 0.0028$, $p = 0.0109$, $p = 0.0019$) or Flag-CDK9 (**h**) ($p = 0.0050$,

$p = 0.0042$, $p = 0.0135$, $p = 0.0183$). FIC2 cells were treated with DMSO or SGC707 (**i**) ($p = 0.0007$, $p = 0.0035$, $p = 0.0014$, $p = 0.00009$). The occupancy of Flag-CycT1 or Flag-CDK9 at LTR-luciferase regions was measured. **j–l** Luciferase activities were measured for Tat transfected (**j**) ($p = 0.0017$, $p = 0.0158$), JQ1 (**k**) ($p = 0.0005$, $p = 0.0065$), or PMA (**l**) ($p = 0.000003$, $p = 0.0011$) treated WT and KO cells when CycT1 overexpression. **m–q** Luciferase activities were measured for Tat transfected (**m**) ($p = 0.0005$, $p = 0.0041$), JQ1 (**n**) ($p = 0.0033$, $p = 0.0137$), or PMA (**o**) ($p = 0.0042$, $p = 0.0019$) treated cells overexpression CycT1 when treated with SGC707, in WT, CDK9 KD cells ($p = 0.0147$, $p = 0.0099$, $p = 0.0270$) (**p**), or in NH1 cells transfected with indicated plasmid together with Tat (**q**) ($p = 0.0008$, $p = 0.0025$, $p = 0.0003$). Error bars = mean \pm SD of three biological replicates. * $p < 0.05$, ** $p < 0.01$, *** $p < 0.001$, n.s. denotes no significance, two-tailed t test except (**f**) was assessed by Wilcoxon's test. Source data are provided as a Source Data file.

These data suggested that PRMT3 promotes the TEAD4 binding at the LTR.

In light of the above results, we next assessed the combinatorial effects of PRMT3 and TEAD4 on Tat-dependent HIV-1 transcription by measuring luciferase signals in NH1 cells co-transfected with plasmids expressing both TEAD4 and PRMT3 or either alone. The data showed that the co-expression of both proteins resulted in a higher level of activation compared to either alone (Fig. 5n), indicating that the two proteins cooperate to increase HIV-1 transcription. As a potential explanation of this cooperativity, we found that the TEAD4 overexpression led to a significantly enhanced association of PRMT3 at the LTR (Fig. 5o), while TEAD4 knockdown resulted in a significant decrease in PRMT3's binding at the LTR-luciferase reporter region (Fig. 5p), suggesting that TEAD4 promotes the PRMT3 binding.

In addition to the HIV-1 LTR, we asked whether this PRMT3-TEAD4 mutual promotion and co-localization also occur on host genes. To address this, we conducted ChIP-qPCR to examine the presence of TEAD4 at the loci, including *PRDM1*, *SLITRK5*, and *TGFB2*, where we previously detected the PRMT3 occupancy. Indeed, TEAD4 binding was detected at the promoters of all three examined host genes (Supplementary Fig. 13a–c), which was significantly decreased in PRMT3 KO cells or cells exposure to PRMT3 inhibitor treatment (Supplementary Fig. 14a–f), expanding the relevance of our findings beyond HIV-1 to potentially include cooperative PRMT3/TEAD4 transcriptional regulation of host genes. Together, these findings collectively reveal a cooperative activation of HIV-1 transcription, as well as a small subset of host genes, by PRMT3 and TEAD4, which apparently results from the mutual promotion of bindings to a common motif.

PRMT3 interacts with TEAD4 and P-TEFb to form a transcriptional hub that co-localizes in the nucleus

In light of the above results showing co-localization of PRMT3 and TEAD4 at the LTR, resulting in their cooperative activation of HIV-1, we examined whether PRMT3 physically interacts with TEAD4. Indeed, co-IP experiments revealed a strong interaction between the two (Fig. 6a, b). The interaction between PRMT3 and TEAD4 was also demonstrated in the GST pull-down assay (Fig. 6c). Furthermore, consistent with the earlier demonstration that Tat promotes TEAD4's binding at the LTR-luciferase reporter region (Fig. 5g), the co-IP experiments showed that Tat also interacts with TEAD4 (Fig. 6d, e), again supporting a Tat-dependent mechanism for HIV-1 transactivation by TEAD4.

As both PRMT3 and TEAD4 regulate HIV-1 transcription in a Tat-dependent manner, and HIV-1 transcription is known to be highly dependent on the Tat/P-TEFb complex^{35,38,46}, we also examined whether PRMT3 and TEAD4 both interact with P-TEFb. Co-IP experiments revealed clear signal of both CycT1 and CDK9 in the pull-down products upon immunoprecipitation of Flag-PRMT3 (Fig. 6f). Consistent with this result, PRMT3 was present in the immunoprecipitation products of Flag-CycT1 (Fig. 6g). Furthermore, we performed reciprocal co-IPs using Myc-TEAD4 or Flag-CycT1 as the bait to test whether

TEAD4 and P-TEFb can also interact with each other. The data in Fig. 6h and i indicate that in addition to pulling down PRMT3, both TEAD4 and CycT1 were able to co-precipitate each other. Furthermore, the interaction among PRMT3, TEAD4, and P-TEFb was also demonstrated by performing endogenous IP (Fig. 6j–l).

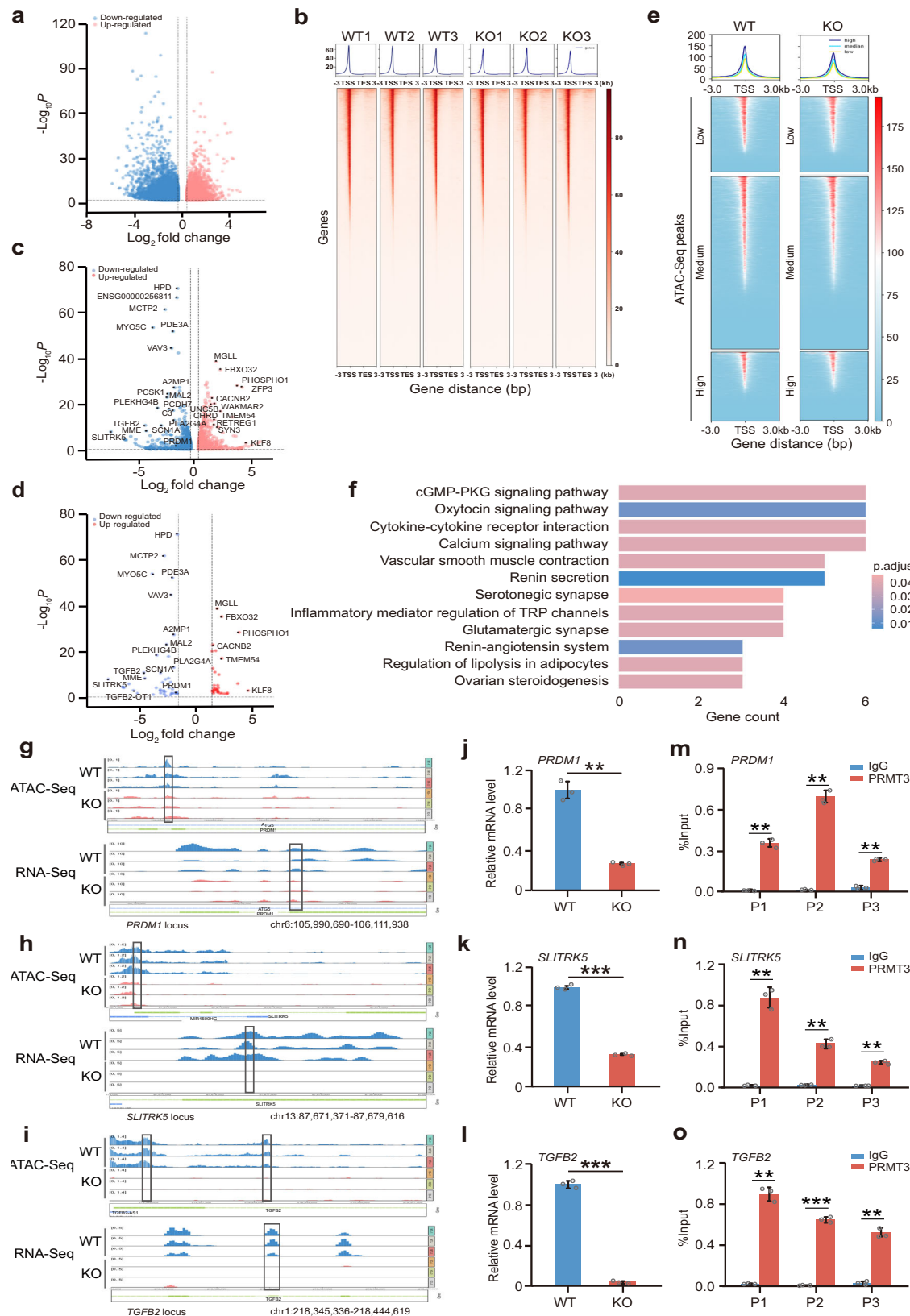
The above co-IP results have revealed physical interactions that exist among PRMT3, TEAD4, and P-TEFb. To validate this conclusion, we performed immunofluorescence staining and found that PRMT3, TEAD4, and CycT1 demonstrated pairwise partial co-localization in the nucleus (Fig. 6m). Collectively, these biochemical and cell biology results support a scenario wherein PRMT3 modifies chromatin to form a nuclear transcriptional hub that also contains TEAD4 and P-TEFb for transcriptional activation and latency reversal of HIV-1 (Fig. 7).

Discussion

The elusive nature of latent HIV-1 reservoirs presents a formidable challenge to eradicating the virus from infected individuals^{49–51}. Despite the various strategies employing either the latency reversal agents (LRAs) or latency promoting agents (LPAs), which are aimed at either purging or deeply silencing the latent viral reservoirs, these agents have yet to be made into effective drugs for curing HIV/AIDS and targets are still needed for the development of therapies. Furthermore, the premise of using the current and future versions of LRAs or LPAs for treating HIV-1 hinges on the potential to epigenetically modulate the HIV-1 promoter activity, aiming for a sustained activation or suppression of viral transcription, respectively^{52–54}. The significance of targeting epigenetic control of viral transcription was highlighted recently in a human clinical trial, where the combination of panobinostat, a potent pan-histone deacetylase inhibitor, with interferon- α 2a resulted in an enhanced vulnerability of latent HIV-1 reservoir cells, underscoring the pivotal role of epigenetic manipulation in combating HIV-1 persistence².

In the current study, by performing the dCas9-targeted LTR interactome screening, we have identified PRMT3 as a positive regulator to promote HIV-1 latency reversal. Mechanistically, PRMT3 activates HIV-1 transcription by interaction with TEAD4 and the two proteins co-localize at the LTR by using specific TEAD4-binding motifs, thereby regulating chromatin accessibility and facilitating P-TEFb/Tat recruitment. Thus, our findings propose a promising epigenetic strategy to combat latent HIV-1 infection, underscoring PRMT3 and its partners as promising therapeutic targets for anti-HIV-1 drug development.

Our study demonstrates TEAD4 as a positive regulator of HIV-1 transcription, acting alongside PRMT3 through a specific interaction with the LTR's GGAAT motif. This discovery expands our current understanding of TEAD4's regulatory roles in host cells and suggests its potential regulation of HIV-1 viral expression. The specificity of TEAD4's interaction with the motif containing the core GGAAT sequence within the HIV-1 LTR and its synergy with PRMT3 in promoting Tat-dependent HIV-1 transcription and a specific subset of host gene transcription is particularly intriguing given TEAD4's established roles in cell survival, proliferation, tissue regeneration, stem cell



maintenance, embryonic trophoblast and organ development and tumorigenesis^{9,11,13,14,55}. Specifically, we selected three host genes, *PRDM1*, *SLITRK5*, and *TGFB2*, for further validation of our proposed PRMT3-TEAD4 regulation model. Our data demonstrate that in addition to the HIV-1 LTR, PRMT3 and TEAD4 indeed associated with these cellular gene promoters, where the binding of TEAD4 significantly

decreases after the depletion of PRMT3, suggesting a common regulatory mechanism involving the PRMT3-TEAD4 complex that exists at the HIV-1 LTR, as well as the promoters of selected host genes. At the HIV-1 LTR, the interaction of the PRMT3-TEAD4 complex with Tat and the P-TEFb provides further regulation of HIV-1 transcription. On cellular gene promoters such as the three genes mentioned above, it is

Fig. 4 | PRMT3 affects chromatin accessibility and transcription of a subset of host genes. **a** The Volcano plot displays the differential loci in WT and PRMT3 KO cells. The x-axis value indicates the log₂ fold change of average density of peaks in WT and KO cells. The y-axis value indicates $-\log_{10}P$. The dotted line represents $p = 0.05$. **b** A heatmap showing the distribution of accessible regions upstream of the TSS and downstream of the TES identified by ATAC-seq using three biological replicates of WT and KO cells. **c** The Volcano plot showing differentially expressed genes, down-regulated (blue) and up-regulated (red), in WT and KO cells using RNA-seq. **d** The Volcano map was used to display the genes with differential transcription level and chromatin accessibility in WT and KO cells from the combining analysis of ATAC-Seq and RNA-Seq results. **e** The plot (Up) displayed the normalized ATAC-Seq signal of three sets of genes, and the heatmaps (Down) showed the ATAC-seq signal for each gene that displayed in a row. **f** The related signaling pathway of PRMT3-

regulated genes showed by KEGG analysis. **g–i** Representative tracks of ATAC-seq (WT: blue; KO: pink) and RNA-Seq (WT: blue; KO: pink) signals showing decreased ATAC-Seq signals along with decreased RNA-seq signals within *PRDM1*, *SLITRK5*, and *TGFB2* regions in KO cells compared to those in WT cells. The boxed area indicates the representative decreased areas. The schematics for the three genes were displayed at the bottom of the figure (green). **j–l** RT-qPCR analysis showed the expression of three representative genes in WT and KO cells (**j**: $p = 0.0054$, **k**: $p = 0.0005$, **l**: $p = 0.0002$). *GAPDH* was used for normalization in the RT-qPCR. **m–o** ChIP-qPCR analysis detected PRMT3's association with three regions of the promoters (P1-P3) of selected genes (**m**: $p = 0.0032$, $p = 0.0016$, $p = 0.0038$, **n**: $p = 0.0047$, $p = 0.0043$, $p = 0.0037$, **o**: $p = 0.0019$, $p = 0.0004$, $p = 0.0061$). Error bars = mean \pm SD of three biological replicates. * $p < 0.05$, ** $p < 0.01$, *** $p < 0.001$, two-tailed t test. Source data are provided as a Source Data file.

conceivable that transcription can also be modulated through controlling the function and/or binding of the PRMT3-TEAD4 complex to the GGAAT motif in response to changes in physiological or pathological conditions. This co-regulation of viral and host gene transcription by PRMT3-TEAD4 underscores a finely tuned regulatory mechanism that integrates the cellular and viral transcriptional control. Furthermore, TEAD4 has also been demonstrated to interact with P-TEFb, which is the core transcriptional component of the Super Elongation Complex (SEC) essential for Tat-activated HIV-1 transcription. Given the fact that TEAD4 is a DNA sequence-specific transcription factor, it remains to be investigated whether it plays a key role in recruiting SEC to both host and HIV-1 gene promoters that contain the TEAD4-binding motif.

While previous studies have indicated PRMT3's involvement as a key factor in mediating host responses to viral infection^{17,30}, its specific role in HIV-1 infection and latency remains largely unexplored. For instance, in zebrafish, PRMT3 has been shown to negatively regulate antiviral responses¹⁷. Similarly, recent studies utilizing the PRMT3 inhibitor, SGC707 treatment, or PRMT3 knockout mice have revealed PRMT3's facilitation of HSV-1 infection³⁰. In conjunction with our current discovery demonstrating PRMT3's promotion of HIV-1 transcription to reverse latency, these findings suggest that PRMT3 may serve as a potential target for broad-spectrum antiviral drugs. However, future comprehensive research is imperative to fully comprehend the extent of PRMT3's involvement in mediating viral-host interactions.

It is noteworthy that besides PRMT3, other PRMTs have also been implicated in regulating anti-HIV activity. For instance, PRMT6 has been shown to inhibit HIV-1 replication in vitro by directly methylating several HIV-1 proteins, including Tat, Rev, and nucleocapsid protein, thereby interfering with their functions^{56,57}. Similarly, PRMT2 was recently discovered to suppress HIV-1 transcription by methylating Tat and promoting the phase separation of P-TEFb and Tat⁵⁸. Thus, in addition to PRMT3, other members of the PRMT family should be explored as potential targets for developing effective antiviral drugs.

In addition to its effects on viral gene expression, PRMT3's regulation of host gene transcription has been implicated in various cellular processes, including tumorigenesis, oxaliplatin resistance in liver cancer, retinoic acid signaling, and hepatic lipogenesis^{18,20,28,29,59,60}. However, the precise mechanism(s) underlying these transcriptional effects of PRMT3 remain unclear. In this study, the comparison of ATAC-Seq and RNA-Seq data between WT and PRMT3 KO cells reveals that PRMT3 selectively regulates chromatin accessibility and transcription of a small subgroup of human genes, including some well-studied genes such as *TGFB2*, which is relevant to the potential pathogenic effects of PRMT3 in tumorigenesis. The selectivity of PRMT3's action is apparently achieved through forming a complex with TEAD4, which then co-localizes at specific gene promoter regions via binding to the TEAD4-recognition motif. Together, these findings have revealed the mechanistic basis for PRMT3's control of the transcription of HIV-1 and a selected group of host genes.

Although the PRMT3-created transcription hub containing TEAD4 and P-TEFb is demonstrated in the current study as important for HIV-1 to escape latency, it is presently unknown whether it also plays a role during the establishment of latency. It is conceivable that the loss of expression/function of any component of the hub could be responsible in this latter process. Further studies are thus necessary to test this hypothesis and explore the possibility of targeting the PRMT3 transcription hub to cure HIV/AIDS.

Methods

Ethics statement

The HIV-positive patient's sample collection was approved by the Fifth Medical Center of the Chinese PLA General Hospital (KY-2023-10-67-1). The committee approved the experiments and confirmed that all experiments conform to the relevant regulatory standards. The informed consent was obtained from all the patients for the publication of data in this study.

Cell culture, plasmids and antibodies

NH1, PRMT3 KO, HeLa, HEK293T, FIC2, and CDK9 KD cells were cultured in Dulbecco's modified Eagle's medium (DMEM; BI) supplemented with 10% fetal bovine serum (FBS) (Corning), 1% penicillin-streptomycin at 37 °C with 5% CO₂. Jurkat 2D10 and MT4 cells were cultured in RPMI 1640 with 10% FBS and 1% penicillin-streptomycin at 37 °C with 5% CO₂. For HeLa cell and HEK293T cell expression, DNA was transfected with polyethylenimine (PEI) (Polysciences). All transfections were performed according to the manufacturer's protocol. The Luciferase Reporter Assay System was purchased from Promega. Primers, plasmids, and antibodies are listed in Supplementary Data 4, 5.

In vitro dCas9-3×Flag/sgRNAs complex formation

sgRNAs synthesis were transcribed by using HiScribe™ Quick T7 High Yield RNA Synthesis Kit (NEB) in vitro following the instructions. The plasmid PCT310 containing dCas9-3 × Flag was obtained from Robert Tjian Lab as a gift³⁴. GST-tagged dCas9-3 × Flag was expressed and purified by using the *E. coli* BL21 expression system slightly modified from the previous study³⁴. The product was eluted from Ni-NTA resin by using elution buffer [500 mM NaCl, 20 mM Tris (pH7.5), 5% glycerol, 200 mM imidazole, 20 mM 2-mercaptoethanol] and analyzed by running the SDS-PAGE and followed by Coomassie Blue Staining. Protein was aliquoted and stored at -80°C . Then, the complex formation was performed by incubating 2.5 μg sgRNAs with 10 μg dCas9-3 × Flag in 200 μl reaction volume at a molar ratio of 3:1 at room temperature for 1 h.

dCas9-targeted LTR proteome analysis

One million NH1 cells with an integrated with HIV-1 5' LTR-driven luciferase reporter construct, which contains 424 bp of LTR. Cells were fixed with 1% formaldehyde for 15 min at room temperature and 0.125 M Glycine for 5 min to quench unreacted formaldehyde at room

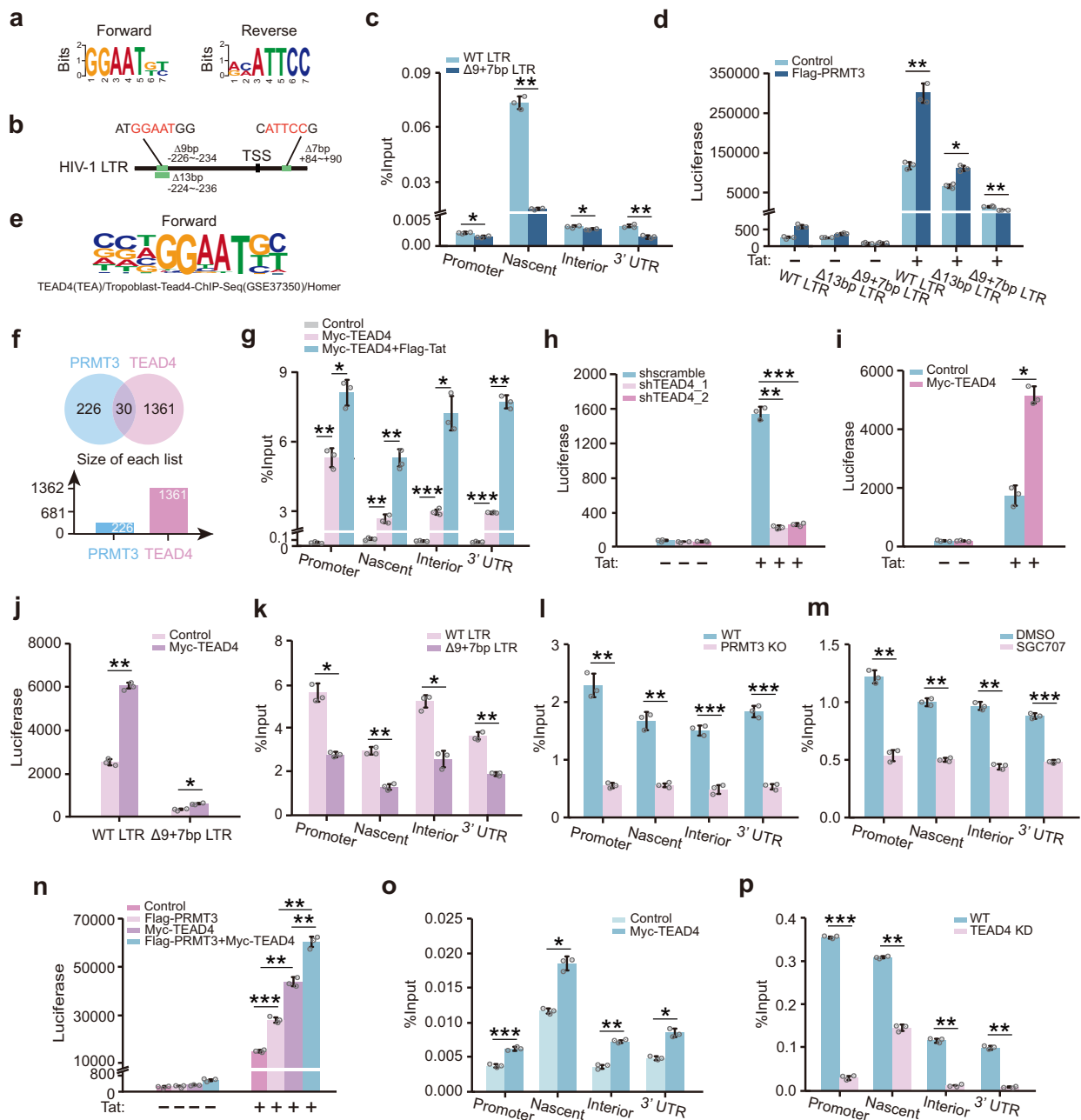


Fig. 5 | PRMT3 co-localizes with TEAD4 at LTR for their synergistic activation of HIV-1 transcription through a motif containing the GGAAT core sequence.

a DREME enrichment analyses of ATAC-seq in WT and PRMT3 KO cells. **b** GGAAT-motif location in LTR mutants. **c** PRMT3's occupancy at LTR-luciferase regions in cells transfected with WT or Δ9 + 7 bp LTR-luciferase reporter ($p = 0.0108$, $p = 0.0020$, $p = 0.0100$, $p = 0.0013$) was measured. **d** Luciferase activities were measured in cells cotransfected with WT or mutant LTR-luciferase reporter together with control or Flag-PRMT3 plasmid with or without Tat ($p = 0.0056$, $p = 0.0158$, $p = 0.0091$). **e** The reported TEAD4 binding motif. **f** Venn diagram of PRMT3- against TEAD4-associated genes. **g** Myc-TEAD4's occupancy at LTR-luciferase regions ($p = 0.0029$, $p = 0.0425$; $p = 0.0026$, $p = 0.0029$; $p = 0.0006$, $p = 0.0184$; $p = 0.0001$, $p = 0.0015$) in cells with or without Tat was measured. **h–j** Luciferase activities were measured in NH1 cells transfected with shRNAs targeting TEAD4 (**h**) ($p = 0.0020$, $p = 0.0009$), the plasmid expressing Myc-

TEAD4 (**i**) ($p = 0.0134$), or in HeLa cells cotransfected with WT or Δ9 + 7 bp LTR construct together with Myc-TEAD4 and Tat ($p = 0.0017$, $p = 0.0291$) (**j**). **k–m** Myc-TEAD4's occupancy at LTR-luciferase regions in cells transfected with WT or Δ9 + 7 bp LTR (**k**) ($p = 0.0110$, $p = 0.0053$, $p = 0.0262$, $p = 0.0032$), or in WT and KO cells (**l**) ($p = 0.0090$, $p = 0.0067$, $p = 0.00006$, $p = 0.0007$), or in cells treated with DMSO or SGC707 (**m**) ($p = 0.0016$, $p = 0.0034$, $p = 0.0019$, $p = 0.0005$) was measured. **n** Luciferase activities were measured in cells cotransfected with Myc-TEAD4 and Flag-PRMT3 ($p = 0.0046$, $p = 0.0059$) versus cells transfected with either alone ($p = 0.0006$, $p = 0.0037$). **o**, **p** PRMT3's occupancy at LTR-luciferase regions with or without TEAD4 overexpression (**o**) ($p = 0.0007$, $p = 0.0104$, $p = 0.0061$, $p = 0.0122$), or knockdown (**p**) ($p = 0.00003$, $p = 0.0016$, $p = 0.0016$, $p = 0.0013$) was measured. Error bars = mean \pm SD of three biological replicates. $*p < 0.05$, $**p < 0.01$, $***p < 0.001$, two-tailed t test. Source data are provided as a Source Data file.

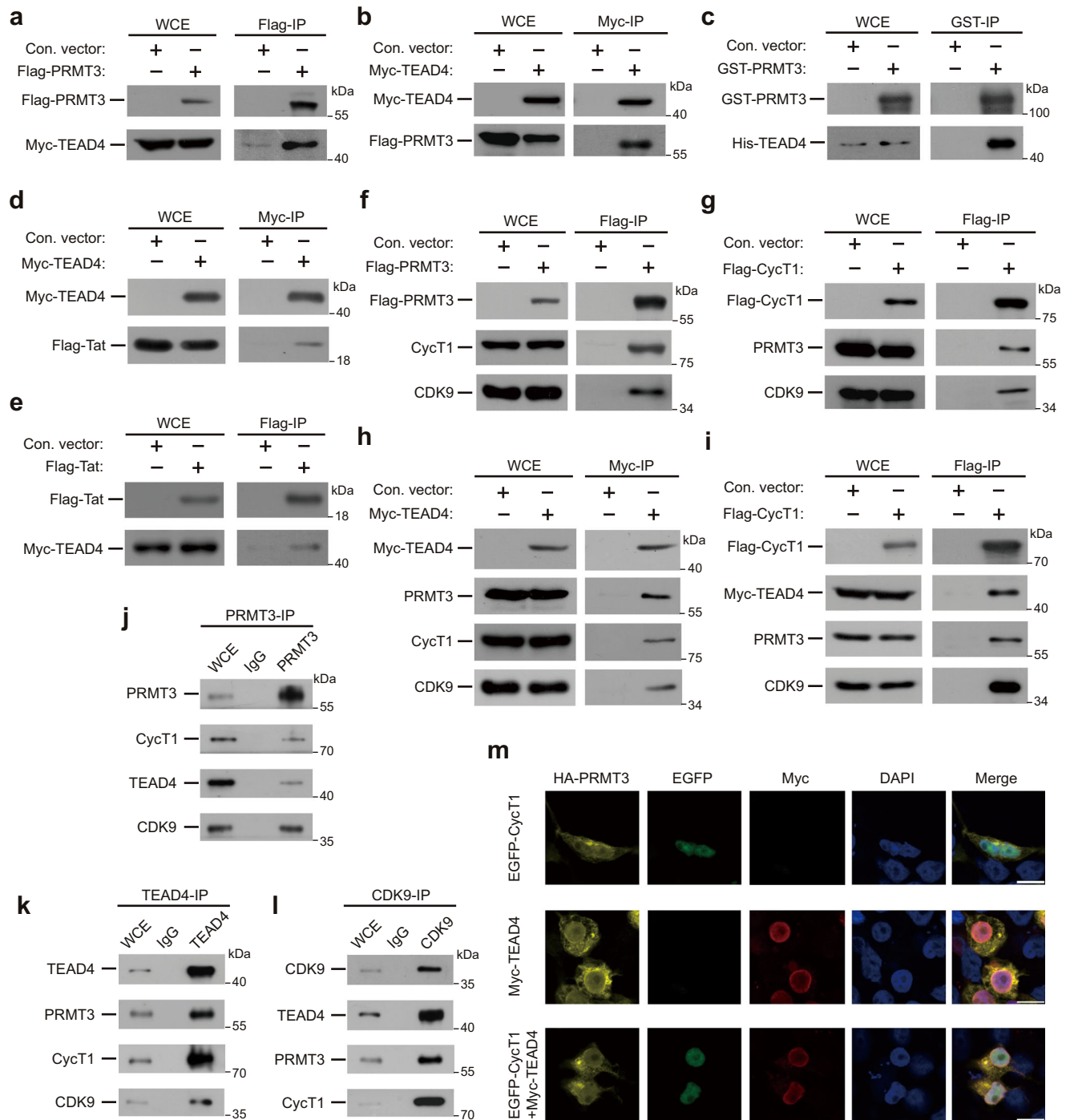


Fig. 6 | PRMT3 interacts with TEAD4 and P-TEFb to form a transcriptional hub that co-localizes in the nucleus. **a, b** HEK293T cells were cotransfected with empty vector or Flag-PRMT3 with Myc-TEAD4 (**a**), or Myc-TEAD4 with Flag-PRMT3 (**b**) for 40 h. Flag-PRMT3 (**a**) or Myc-TEAD4 (**b**) was immunoprecipitated using anti-Flag antibody or anti-Myc antibody, following with western blot analysis for the indicated protein. **c** GST pull-down assay was performed using GST-PRMT3 and His-TEAD4 that were purified from *E. coli*. The products from the pull-down assay were subjected to western blot analysis for the detection of the indicated proteins. **d, e** HEK293T cells that were cotransfected with empty vector or plasmid expressing Myc-TEAD4 together with Flag-Tat (**d**), or plasmid expressing Flag-Tat together with Myc-TEAD4 (**e**) for 40 hours. Myc-TEAD4 (**d**) or Flag-Tat (**e**) was immunoprecipitated using anti-Myc or anti-Flag IP, following with western blot analysis for the indicated protein. **f, g** Whole cell lysates of HEK293T cells that were transfected with empty vector or plasmid expressing Flag-PRMT3 (**f**), or plasmid

expressing Flag-CycT1 (**g**) for 40 h were used for anti-Flag IP, following with western blot analysis for the indicated protein. **h, i** Whole cell lysates of HEK293T cells that were transfected with empty vector or plasmid expressing Myc-TEAD4 (**h**), or plasmid expressing Flag-CycT1 together with Myc-TEAD4 (**i**) for 40 h were used for anti-Myc (**h**) or anti-Flag (**i**) IP following with western blot analysis for the indicated protein. **j–l** Whole cell lysates of HeLa cells was used for chromatin pellets collection with lysis buffer and immunoprecipitated using anti-IgG, anti-PRMT3, anti-TEAD4, or anti-CDK9 antibody, following with western blot analysis for the indicated protein. **m** HEK293T cells were cotransfected with plasmids expressing HA-PRMT3 together with EGFP-CycT1 (green), Myc-TEAD4, or EGFP-CycT1 + Myc-TEAD4 for 40 h. Protein localization was detected by immunofluorescence using anti-HA antibodies (yellow) or anti-Myc antibodies (red), and 40,6-diamidino-2-phenyl-indole (DAPI) (nuclei, blue) for confocal microscopy analysis. Scale bars, 10 μ m. All western blots are representative of three independent experiments.

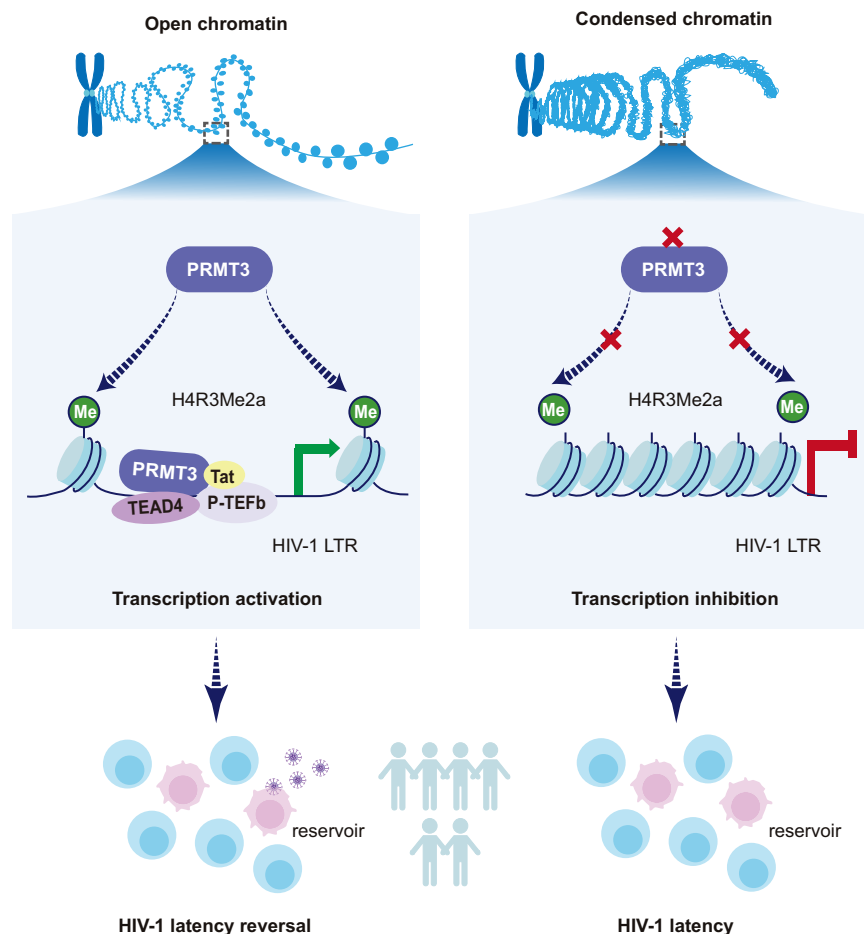


Fig. 7 | The hypothesis model of PRMT3's role in the regulation of HIV-1 transcription and latency reversal. PRMT3 increases chromatin accessibility by elevating H4R3Me2a level to form a transcriptional hub containing TEAD4, P-TEFb, and Tat at the HIV-1 promoter for viral transcription and latency reversal.

temperature. Use 20 ml of cold PBS to wash cells twice. Scrape cells with 2 ml cold PBS containing protease inhibitor and dithiothreitol (DTT). Spin at $700 \times g$ at 4°C for 3 min to pellet cells. Cells were lysed with lysis buffer [1% SDS, 10 mM EDTA, 50 mM Tris, pH 8.1] and incubated on ice for 20 min. Cells were sheared with a Covaris sonicator M220 until genomic DNA was visualized to be at 200–1000 bp. The DNA was cleared with a high-speed spin ($15,000 \times g$ for 10 min) at 4°C . The DNA was diluted by ChIP Dilution Buffer [0.01% SDS, 1% Triton X-100, 1.2 mM EDTA, 16.7 mM Tris-HCl, pH 8.1, 167 mM NaCl]. dCas9-3 \times Flag/sgRNAs complex was added to the sheared DNA and incubated at 4°C overnight. The anti-Flag M2 agarose resin (Sigma) was added, followed by a 3 h incubation at 4°C . The resin was spun down at $1500 \times g$ at 4°C for 1 min and washed with high salt wash buffer [0.1% SDS, 1% Triton X-100, 2 mM EDTA, 20 mM Tris-HCl, pH 8.1, 300 mM NaCl] for once, low salt wash buffer [0.1% SDS, 1% Triton X-100, 2 mM EDTA, 20 mM Tris-HCl, pH 8.1, 150 mM NaCl] for three times, and TE buffer [10 mM Tris-HCl, 1 mM EDTA, pH 8.0] for twice, with each wash for 5 min rotated at 4°C . The products concentrated by beads were used for subsequent experiments.

Mass spectrometry (MS) and analysis

The sample of dCas9-3 \times Flag-sgLTRs and dCas9-3 \times Flag-sgGal4 (control) immunoprecipitated proteins were prepared and analyzed by MS. In general, the eluted LTR binding proteins were reduced in 20 mM DTT at 95°C for 5 min, and subsequently alkylated in 50 mM iodoacetamide for 30 min in the dark at room temperature. After alkylation, the samples were transferred to a 10 kD centrifugal spin filter (Millipore) and sequentially washed with 200 μl of 8 M urea for

three times and 200 μl of 50 mM ammonium bicarbonate for two times by centrifugation at $14,000 \times g$. Next, tryptic digestion was performed by adding trypsin at 1:50 (enzyme/substrate, m/m) in 200 μl of 50 mM ammonium bicarbonate at 37°C for 16 hours. Peptides were recovered by transferring the filter to a collection tube and spinning at $14,000 \times g$. To increase the yield of peptides, the filter was washed twice with 100 μl of 50 mM ammonium bicarbonate. Peptides were desalted by StageTips.

MS experiments were performed on a nanoscale EASY-nLC 1200 UHPLC system (Thermo Fisher Scientific) connected to an Orbitrap Fusion Lumos equipped with a nanoelectrospray source (Thermo Fisher Scientific). Mobile phase A contained 0.1% formic acid (v/v) in water; mobile phase B contained 0.1% formic acid in 80% acetonitrile (ACN). The peptides were dissolved in 0.1% formic acid (FA) with 2% acetonitrile and separated on an RP-HPLC analytical column (75 $\mu\text{m} \times 25 \text{ cm}$) packed with 2 μm C18 beads (Thermo Fisher Scientific) using a linear gradient ranging from 5% to 22% ACN in 90 min and followed by a linear increase to 35% B in 20 min at a flow rate of 300 nl/min. The Orbitrap Fusion Lumos acquired data in a data-dependent manner, alternating between full-scan MS and MS2 scans. The spray voltage was set at 2.2 kV, and the temperature of the ion transfer capillary was 300°C . The MS spectra (350–1500 m/z) were collected with 120,000 resolutions, AGC of 4×10^5 , and 50 ms maximal injection time. Selected ions were sequentially fragmented by HCD with 30% normalized collision energy, specified isolated windows 1.6 m/z, and 15,000 resolutions. AGC of 5×10^4 and 40 ms maximal injection time were used. Dynamic exclusion was set to 40 s. Unassigned ions or those with a charge of 2+ and >7+ were rejected for MS/MS.

Raw data was processed using Proteome Discoverer (PD, version 2.4), and MS/MS spectra were searched against the reviewed SwissProt human proteome database. Only peptides with at least six amino acids in length were considered. The peptide and protein identifications were filtered by PD to control the false discovery rate (FDR) <1%. At least one unique peptide was required for protein identification.

Generation of stable knockout cell line

sgRNA sequence was ligate into plasmid pSpCas9 (BB)–2A-Puro (PX459), which was purchased from Addgene (#48139). Cells were transfected with the plasmid expressing sgPRMT3 by using Lipofectamine 3000 (Invitrogen) according to the manufacturer's protocol. After 48 h of transfection, cells that did not contain the plasmid were killed with puromycin for 2 days, then changed into DMEM with no antibiotics and plated into 96-well plate for single clone selection. After verification with western blot, the genome was extracted and sent for sequencing.

Co-Immunoprecipitation (co-IP) and western blot

HEK293T cells were transfected with 15 µg of total plasmid DNA encoding Flag-tagged or Myc-tagged bait protein by using PEI. After 48 h, cells were collected, lysed by resuspended with 1 ml whole cell lysis buffer [20 mM HEPES (pH 7.9), 150 mM NaCl, 1.5 mM MgCl₂, 5% Glycerol, 0.5 mM EDTA, 0.1% NP40] and incubated for 30 min at 4 °C by gentle rotating. The supernatant was collected by centrifuging the cells at 19,000 × g for 10 min for twice. 20 µl M2 agarose resin (Sigma) or anti-Myc agarose beads (Lablead) were added to each reaction volume and incubated overnight at 4 °C. The resin was collected by centrifuging at 1500 × g at 4 °C for 1 min and washed with high salt wash buffer [20 mM HEPES (pH 7.9), 300 mM KCl, 10% Glycerol, 0.2 mM EDTA, 0.2% NP40] for once, low salt wash buffer [20 mM HEPES (pH 7.9), 100 mM KCl, 10% Glycerol, 0.2 mM EDTA, 0.2% NP40] for three times. Then, IP products were boiled with 1× SDS loading buffer at 100 °C for 10 min. Samples were loaded on an SDS-PAGE gel and transferred to membranes for WB analysis. The endogenous IP was performed as previously described⁶¹. Cells were subjected to chromatin fractionation prior to immunoprecipitation. Cells were lysed in EBC-150 buffer (50 mM Tris, pH 7.5, 150 mM NaCl, 0.5% NP-40, 2 mM MgCl₂, supplemented with protease and phosphatase inhibitor cocktails) for 20 min at 4 °C, followed by centrifugation to remove cytoplasmic proteins. Subsequently, the chromatin fraction was solubilized in EBC-150 buffer with 500 U/ml Benzonase and antibody recognizing PRMT3, TEAD4, or CDK9 for 1 h at 4 °C under rotation. Next, the NaCl concentration of the lysis buffer was increased to 300 mM, and lysates were incubated for another 30 min at 4 °C. The lysates were cleared from insoluble chromatin and were subjected to immunoprecipitation with protein A agarose beads (Millipore) for 1.5 h at 4 °C. The beads were then washed 4–6 times with EBC-300 buffer (50 mM Tris, pH 7.5, 300 mM NaCl, 0.5% NP-40, 1 mM EDTA) and boiled in sample buffer. Bound proteins were resolved by SDS-PAGE and immunoblotted with the indicated antibodies.

Luciferase assay

NH1, a HeLa-based cell line, which contains an integrated HIV-1 LTR fused with a luciferase reporter gene in the genome was used for evaluation of HIV-1 transcription³⁷. Cells were seeded into 12-well plates at a density of 1 × 10⁵ per well and cultured for 24 h. Then, control plasmid, plasmids expressing target protein, shRNA were transfected in to NH1 cells or HeLa cells together with HIV-1 LTR. For drug treatment, the WT NH1 cells or PRMT3 KO cells were treated with JQ1 (5 µM) or PMA (200 nM) or with these reagents in combination with SGC707 (0.25 mM) for 22 h. Each sample was performed in biological triplicates. 48 h later, cells were collected and lysed with 5× lysis buffer in the kit (Promega). Cells were put into –80 °C for at least 2 h and vortex for 15 s. The supernatant was tested for luciferase activity.

Measurement of cell growth

Cell growth was measured using CellTiter-Glo® Luminescent Cell Viability Assay following the instruction as described in the kit (Promega). Prepare WT NH1 and PRMT3 KO cells with medium on a 96-well plate with opaque walls for 100 µl/well. Equilibrate the plate and its contents to room temperature, which will take about 30 min. Each well was supplemented with 100 µl CellTiter-Glo reagents. Mix the contents on an orbital shaker for 2 min to induce cell lysis. Incubate the plate at room temperature for 10 min to stabilize the luminescent signal values, and detect the luminescence signal.

Cell sorting and drug treatment

Peripheral blood mononuclear cells (PBMCs) were isolated from whole blood using a density gradient centrifugation over the Ficoll medium (TBDScience). CD4⁺ T cells were isolated from PBMCs using the Easy-Sep negative-selection Human CD4⁺ T Cell Enrichment Kit (STEMCELL Technologies) according to the manufacturer's instructions after stabled for 3 hours in RPMI 1640 medium (Gibco) containing 10% FBS, 1% penicillin-streptomycin, 2 mM L-glutamine, IL-2 (10 ng/ml), and phytohemagglutinin (1 µg/ml). CD4⁺ T cells were treated with JQ1 (5 µM) or PMA (200 nM) or with these reagents in combination with SGC707 (0.25 mM) for 22 h. Detailed information on the patients is shown in Supplementary Data 6.

Nucleofection in MT4 and primary CD4⁺ T cells

Nucleofection in MT4 cells and human primary CD4⁺ T cells were performed as previously described⁶². MT4 and primary CD4⁺ T cells were counted at 2 × 10⁶/well and suspended with 100 µl transfection buffer (82 µl of Nucleofector® Solution + 18 µl of supplement, Lonza Nucleofector SF Kit for MT4 cell, Lonza P3 Primary Cell Kit for primary CD4⁺ T cells) containing 300 nM of siRNA. The mixture of cells and siRNA were resuspended and transferred to the Nucleocuvette™ Vessels. Cells were subjected to nucleofection using 4D-Nucleofector® X Unit-Lonza Electrotransfer Instrument with program CA137 for MT4 cells and program EH100 for primary CD4⁺ T cell. After nucleofection, 200 µl Opti-MEM was added and incubated for 10 minutes at 37 °C. The samples were gently resuspended and transferred to 12-well plates, and incubated with culture medium for 48 h.

HIV-1 infection of MT4 or TZM-bl cells

The virus suspension was prepared with fresh 1640 cell culture medium. Cells were infected with HIV-1 at a multiplicity of infection (MOI) of 0.005, gently mixed. The virus-cell suspension was transferred to a 24-well plate culture plate, and cultured at 37 °C, 5% CO₂. WT and PRMT3 KO TZM-bl cells were plated at a density of 5 × 10⁶ cells/ml the day before viral infection. Cells were infected with HIV-1 CRF01-AE or NL-43 at an MOI of 0.005. For the SGC707 treatment experiment, cells were infected with HIV-1 at an MOI of 0.05. The virus-cell suspension was incubated for 48 h or 72 h before collection. The viral supernatant or cells were collected for measurement of HIV-1 RNA copies, *pol*, *gag* expression, or p24 level.

Quantification of cellular HIV-1 RNA

Total cellular DNA was extracted from patient CD4⁺ T cells using the Qiagen QIA Symphony DNA Mini kit (Qiagen). Magen HiPure Total RNA Plus Mini Kit, respectively, according to the manufacturer's protocols. The SUPBIO total HIV-1 DNA Quantitative PCR Kit was used for the simultaneous quantitation of total HIV-1 DNA and cell numbers. The SUPBIO HIV-1 usRNA Quantitative PCR Kit was used for the quantification of cell-associated HIV-1 RNA. The measurement of relative HIV-1 RNA copies in cells was also performed by quantitation of the *pol* expression and calculation of the viral copies using the standard curve, which was normalized to the expression of *GAPDH*.

ELISA measurement of p24 expression

The p24 expression in the viral supernatant was detected using the lentivirus Titer p24 Assay Kit (EasyQuarter). In general, the HIV p24 standard curve was prepared. 25 μ l of lysis buffer was added to each well, followed by the addition of 75 μ l sample or standard to the appropriate wells. 75 μ l enzyme conjugate was added to the reaction wells and vibrated for 60 seconds, which was then placed at 37 °C for 50 min. Wells were washed with 300 μ l wash buffer for 5 times. Then, 100 μ l of TMB development solution was added to each well and incubated for 10 min at 37 °C. 50 μ l of stop solution was added to each well and vibrated for 60 s. The OD 450 nm was measured.

Chromatin immunoprecipitation (ChIP)-q-PCR assay

The ChIP experiment was performed as previously described with slightly modified^{63–66}. DNA was sheared as described above. Antibodies of control IgG (Cell Signaling Technology) or PRMT3 antibody (Novus) were added to the clean sheared DNA at 4 °C overnight. Dyna beads (Invitrogen) were added the after day and rotated at 4 °C for 3 h. The immune complex was washed by using high salt wash buffer for once, low salt wash buffer for three times, and TE buffer for two times, with each wash for 5 min rotated at 4 °C, and eluted with 200 μ l elution buffer for 1 h. The eluted product was isolated from the resin and added 8 μ l 5 M NaCl for reverse crosslinking at 65 °C for 5 h. Add 1 μ l of RNase A and incubate for 30 min at 37 °C. Then, add 4 μ l 0.5 M EDTA, 8 μ l 1 M Tris-HCl pH 6.5, and 1 μ l Proteinase K and incubate at 50 °C for 4 h. The DNA product was purified by using the Cycle Pure Kit (Omega). The amount of ChIP DNA product at different LTR regions was detected by using q-PCR.

Cleavage Under Targets & Tagmentation (CUT&Tag) sequencing

CUT&Tag was performed following the protocol provided in the Hyperactive Universal CUT&Tag Assay Kit for Illumina Pro (TD904-01, Vazyme). NH1 cells were harvested and counted, and aliquots of 50,000 cells were centrifuged at 600 \times g for 5 min at room temperature. Cells were washed twice in 1.5 ml Wash Buffer with gentle pipetting. A total of 100 μ l of cell (nuclei) suspension was transferred to an 8-strip tube containing activated Con A-coated magnetic beads, mixed by inversion, and incubated at room temperature for 10 min, with occasional mixing (2–3 times by inversion). After a brief centrifugation (<100 \times g), the reaction mix was collected, and the tube was placed on a magnetic separation rack. Once the solution cleared (~2 min), the supernatant was discarded.

Each sample was resuspended in 50 μ l of precooled Antibody Buffer, and 1 μ g of IgG or PRMT3 antibody was added. The mixture was briefly centrifuged to collect the contents at the bottom of the tube and incubated overnight at 4 °C. The primary antibody was removed using the magnet stand, and the cells were incubated at room temperature with a 1:100 dilution of the secondary antibody in 50 μ l of Dig-Wash buffer for 30 minutes with rotation. Unbound antibodies were removed by washing the cells three times for 2 minutes in 0.2 ml Dig-Wash buffer using the magnet stand. For each sample, 2 μ l of pA/G-Tnp Pro was mixed with 98 μ l of Dig-300 Buffer, yielding a final concentration of 0.04 μ M. After removing the liquid on the magnet stand, 100 μ l of the reaction mix was added to the cells and incubated at room temperature for 1 hour with gentle rotation. Unbound pA-Tn5 protein was removed by washing the cells three times for 5 min in 0.2 ml Dig-300 Buffer. Fragmentation was performed by adding 50 μ l of TruePrep Tagment Buffer L to the sample and incubating at 37 °C for 1 h. The sample was briefly centrifuged, and 2 μ l of 10% SDS along with an appropriate amount of DNA Spike-in (adjusted based on target protein abundance and cell input) was added, followed by incubation at 55 °C for 10 min, with mixing 2–3 times by inversion. DNA was purified using DNA extraction beads, and the purified DNA was sent for sequencing.

Raw data of fastq format were processed through in-house perl scripts. Clean data were obtained by removing reads containing

adapter, reads containing ploy-N and low quality reads from the raw data. Clean reads were mapped to the reference genome using Bowtie2 software. Macs2 was used to call peaks with qvalue < 0.05. Peaks were annotated by ChIPseeker package. Differential peak analysis was performed using the DiffBind package (version 3.6.2) in R (version 4.1.2). The DiffBind workflow was initiated by importing the peak files generated by MACS2. The input data were normalized using the “read count” method, and the read counts were then modeled using an edgeR-based negative binomial generalized linear model (GLM) to account for library size differences and overdispersion. Differential peaks were identified using the GLM likelihood ratio test with a false discovery rate (FDR) correction for multiple testing. Peaks with an adjusted *p*-value < 0.05 were considered differentially enriched. All CUT&Tag-seq data analysis was conducted by Beijing SeqWisdom Biotechnology Co., Ltd.

Fluorescence-activated cell sorting (FACS)

The Jurkat-based latency model 2D10 (previously generated by Dr. Jonathan Karn's laboratory⁴³) was used to evaluate the effect on HIV-1 transcription in T cells by PRMT3 inhibitor treatment. 1×10^5 cells were cultured in a 24-well plate and treated with the drug 18 h before cells were collected for FACS analysis. Cells were treated with DMSO or PRMT3 inhibitor SGC707³² together with JQ1 or PMA for HIV-1 transcriptional activation. After 18 h of treatment, cells were collected and then resuspended in cold PBS twice. Quantification of the GFP⁺ cells was performed using a BD FACSCalibur cytometer. Gating strategies were described in the Supplementary Fig. 8. Data were analyzed with the Flowjo software and plotted as bar graphs with error bars representing standard deviations.

GST-Pull down

The GST-pull down assays were performed as previously described^{18,67}. The bacterial expression and purification of GST-tagged PRMT3 and His-tagged TEAD4 were performed as described previously⁶⁸. GSTSep Glutathione MagBeads (Yeasten) were washed twice with the ice-cold interaction buffer (20 mM HEPES, pH: 7.5, 150 mM KCl, 0.2 mM DTT, 1 mM EDTA, and 10% glycerol) and were blocked at 4 °C for 1 h with a blocking buffer (interaction buffer containing 5% BSA). After the blocking step, 40 μ l beads were incubated with the equal volume of GST or GST-tagged PRMT3, respectively, at 4 °C overnight with rotation in the roller. Magnetic beads were collected with magnetic holders and washed with high salt wash buffer [20 mM HEPES (pH 7.9), 300 mM KCl, 10% Glycerol, 0.2 mM EDTA, 0.2% NP40] for once, low salt wash buffer [20 mM HEPES (pH 7.9), 100 mM KCl, 10% Glycerol, 0.2 mM EDTA, 0.2% NP40] for three times. After the washing step, the beads were incubated with His-tagged TEAD4 protein at 4 °C for 3 h with rotation in the roller. Beads were washed with high salt wash buffer for once, low salt wash buffer for three times and boiled with 1 \times SDS loading buffer at 100 °C for 10 min for western blot detection.

ATAC-Seq

Library preparation and sequencing were performed as previously reported⁶⁹. For each library preparation, 5×10^6 WT NH1 cells, PRMT3 KO cells, or cells transfected with a plasmid expressing Tat were used. Cells were washed twice with 500 μ l of ice-cold PBS and then lysed in 1 \times lysis buffer to isolate the nuclei. The TruePrep DNA Library Prep Kit V2 for Illumina and TruePrep Index Kit V2 for Illumina (Vazyme Biotech) were used for library construction. Libraries were purified and selected using AMPure XP beads. The mass concentration of the libraries was determined using a Qubit 3.0 Fluorometer, while the molar concentration was measured with the StepOnePlus™ Real-time PCR system. The lengths of inserted fragments were assessed using the Agilent HS2100 analyzer. The qualified libraries were then sequenced on the Illumina HiSeq X Ten platform in paired-end 150 bp format by Annoroad Gene Technology Co., Ltd.

ATAC-seq data processing

Raw data were stored in FASTQ format, which included the base sequence along with corresponding quality information. Quality control was performed on the raw FASTQ data using Trimmomatic (v0.36). In this step, clean data (clean reads) were generated by removing reads containing adapters, poly-N sequences, and low-quality reads from the raw data. In addition, the Q20, Q30, and GC content of the clean data were calculated. All downstream analyses were based on the high-quality clean data. The clean reads were mapped to the reference human genome using Bowtie2, and the mapping results were visualized using the Integrative Genomics Viewer. Reads with mapping quality below 30, or PCR duplicates, were removed. The remaining high-quality mapped reads were used for further peak calling. Tn5 transposase generates a 9 bp sticky end when cleaving DNA. To improve the accuracy of transposase binding site representation, the reads were adjusted: +4 bp was added to the positive strand and -5 bp was added to the negative strand. Peak calling was performed using the nomodel option with the --shift -75 parameter (shifting the 5' end of each read 75 bp towards the left) and the --extsize 150 parameter (extending the moved reads 150 bp to the right to form the final "virtual fragment").

Motif analysis was performed using HOMER's findMotifsGenome.pl tool. The input files included the peak file and the genome FASTA file. The DNA sequences corresponding to the peaks were extracted and compared with the motif database to identify enriched motifs. Peaks were annotated using the ChIPseeker package. Differential peak analysis was conducted using MANorm, which identifies differential peaks based on peak density. The MANorm workflow was initiated by importing the peak files generated by MACS2. Peaks with an adjusted p -value < 0.05 were considered differentially enriched. All data analysis was conducted by Beijing SeqWisdom Biotechnology Co., Ltd.

RNA-Seq

Total RNA was extracted from 1×10^6 cells (in triplicate) using TRIzol reagents, and genomic DNA was removed with a DNA-free Kit (Thermo Fisher Scientific). RNA library preparation was performed using the VAHTS Universal V6 RNA-seq Library Prep Kit for Illumina, following the manufacturer's instructions. Quality control and sequencing were conducted by Annoroad Gene Technology Co., Ltd.

RNA-seq data processing

RNA-seq data processing was performed as previously described⁶⁹. Low-quality reads and adapter sequences were removed using fqtools. To ensure high-quality data for analysis, a custom Perl script was used to filter the raw data. Reads containing more than 5 base pairs (bp) of adapter sequences were considered contaminated, and if either paired-end (PE) read was contaminated, both reads were discarded. Reads were classified as low quality if more than 15% of their bases had a Phred quality score of ≤ 19 , and if either PE read met this criterion, both reads were removed. Reads with more than 5% ambiguous (N) bases were also discarded, and if one PE read contained excessive N bases, both reads were removed. The reference genome and annotation files were obtained from the ENSEMBL database (<http://www.ensembl.org/index.html>). Genome indexing was performed using Bowtie2 v2.2.3, and clean reads were aligned to the reference genome using HISAT2 v2.1.0. HISAT2, a successor to TopHat2, employs a modified Burrows-Wheeler Transform (BWT) algorithm to improve alignment speed and computational efficiency. Mapping results were visualized using the Integrative Genomics Viewer (IGV) through heatmaps, histograms, scatter plots, or other graphical representations. Differentially expressed genes (DEGs) were identified using the R/Bioconductor package DESeq2, with a Benjamini-Hochberg adjusted p -value < 0.05 and a \log_2 fold-change > 1 as the cutoff. Enrichment analysis was performed using ClusterProfiler, with significance set at adjusted p -value < 0.05 . All RNA-seq data analysis was conducted by Beijing SeqWisdom Biotechnology Co., Ltd.

Immunofluorescence staining and confocal imaging

Cells were seeded on glass coverslips in 24-well plate cotransfected HA-PRMT3 with EGFP-CycT1, Myc-TEAD4, or EGFP-CycT1 and Myc-TEAD4, cells were washed 3 times with PBS for 3 min each time, fixed with 4% paraformaldehyde in PBS for 15 min, permeabilized with 0.2% Triton X-100 in PBS for 30 min at room temperature and blocked with 3% BSA in PBST (0.2% Triton X-100 in PBS) for 30 min at room temperature, then, incubated with primary antibodies overnight at 4 °C. After washes, cells were incubated with Alexa-Fluor-488- or Alexa-Fluor-555-conjugated secondary antibodies (Bioss) for 1 hour at room temperature, and incubated with Hoechst 33342 (Bioss) for 5 min. The coverslips were mounted on glass slides in Mounting Medium and sealed. Immunofluorescence was detected using a Leica confocal microscope. Colocalization of different channels was performed using LAX (Leica).

Statistics and reproducibility

Statistical significance was determined using Origin software 2024b. Sample size, p -values and error bars are described in the text or figure legends. Error bars = mean \pm SD of three biological replicates. A two-tailed Student's t test was conducted using SPSS. $p < 0.05$ (*), $p < 0.01$ (**) and $p < 0.001$ (***) are considered statistically significant. No statistical method was used to predetermine sample size, and no data were excluded from the analyses. All experiments were repeated at least three times, with similar results obtained.

Reporting summary

Further information on research design is available in the Nature Portfolio Reporting Summary linked to this article.

Data availability

All the data in this study is available in the manuscript or supplemental data. The raw data of RNA-Seq and ATAC-Seq generated in this study have been deposited in the NCBI Sequence Read Archive (SRA) database under accession code [PRJNA1125637](https://www.ncbi.nlm.nih.gov/sra/PRJNA1125637). The mass spectrometry proteomics data have been deposited to the ProteomeXchange Consortium [<http://proteomecentral.proteomexchange.org/cgi/GetDataset?ID=PX062187>] via the iProX partner repository under the accession PX062187 or iProX project ID IPX0011474000^{70,71}. Source data are provided in this paper.

References

- Margolis, D. M., Garcia, J. V., Hazuda, D. J. & Haynes, B. F. Latency reversal and viral clearance to cure HIV-1. *Science* **353**, aaf6517 (2016).
- Armani-Tourret, M. et al. Selection of epigenetically privileged HIV-1 proviruses during treatment with panobinostat and interferon- $\alpha 2a$. *Cell* **187**, 1238–1254 (2024).
- Clark, I. C. et al. HIV silencing and cell survival signatures in infected T cell reservoirs. *Nature* **614**, 318–325 (2023).
- Bhardwaj, V. et al. HIV-1 Vpr induces ciTRAN to prevent transcriptional repression of the provirus. *Sci. Adv.* **9**, eadh9170 (2023).
- Li, Y., Liu, X., Fujinaga, K., Gross, J. D. & Frankel, A. D. Enhanced NF- κB activation via HIV-1 Tat-TRAF6 cross-talk. *Sci. Adv.* **10**, eadi4162 (2024).
- Ran, X.-H. et al. TRIM5 α recruits HDAC1 to p50 and Sp1 and promotes H3K9 deacetylation at the HIV-1 LTR. *Nat. Commun.* **14**, 3343 (2023).
- Ne, E. et al. Catchet-MS identifies IKZF1-targeting thalidomide analogues as novel HIV-1 latency reversal agents. *Nucleic Acids Res.* **50**, 5577–5598 (2022).
- Li, C. et al. The chaperone protein p32 stabilizes HIV-1 Tat and strengthens the p-TEFb/RNAPII/TAR complex promoting HIV transcription elongation. *Proc. Natl. Acad. Sci. USA* **120**, e2217476120 (2023).

9. Kumar, N. et al. Host-directed antiviral therapy. *Clin. Microbiol. Rev.* **33**, e00168–19 (2020).
10. Yang, W. et al. RPLP1 restricts HIV-1 transcription by disrupting C/EBP β binding to the LTR. *Nat. Commun.* **15**, 5290 (2024).
11. Yang, X. et al. PEBP1 suppresses HIV transcription and induces latency by inactivating MAPK/NF- κ B signaling. *EMBO Rep.* **21**, e49305 (2020).
12. Dharan, A., Bachmann, N., Talley, S., Zwickelmaier, V. & Campbell, E. M. Nuclear pore blockade reveals that HIV-1 completes reverse transcription and uncoating in the nucleus. *Nat. Microbiol.* **5**, 1088–1095 (2020).
13. Martinat, C. et al. SUMOylation of SAMHD1 at Lysine 595 is required for HIV-1 restriction in non-cycling cells. *Nat. Commun.* **12**, 4582 (2021).
14. Fukuda, H. et al. Cooperative methylation of human tRNA³Lys at positions A58 and U54 drives the early and late steps of HIV-1 replication. *Nucleic Acids Res.* **49**, 11855–11867 (2021).
15. Min, Z. et al. Asymmetrical methyltransferase PRMT3 regulates human mesenchymal stem cell osteogenesis via miR-3648. *Cell Death Dis.* **10**, 581 (2019).
16. Hu, Y., Su, Y., He, Y., Liu, W. & Xiao, B. Arginine methyltransferase PRMT3 promote tumorigenesis through regulating c-MYC stabilization in colorectal cancer. *Gene* **791**, 145718 (2021).
17. Zhu, J. et al. Zebrafish prmt3 negatively regulates antiviral responses. *FASEB J.* **34**, 10212–10227 (2020).
18. Verma, M. et al. PRMT3 interacts with ALDH1A1 and regulates gene expression by inhibiting retinoic acid signaling. *Commun. Biol.* **4**, 109 (2021).
19. Hoekstra, M. et al. Inhibition of PRMT3 activity reduces hepatic steatosis without altering atherosclerosis susceptibility in apoE knockout mice. *Biochim. Biophys. Acta Mol. Dis.* **1865**, 1402–1409 (2019).
20. Kim, D.-i. et al. PRMT3 regulates hepatic lipogenesis through direct interaction with LXR α . *Diabetes* **64**, 60–71 (2015).
21. Huh, K. H. et al. PRMT3: new binding molecule to RhoGDI- α during mycophenolic acid-induced β -cell death. *Transplan. Proc.* **46**, 1229–1232 (2014).
22. Miyata, S., Mori, Y. & Tohyama, M. PRMT3 is essential for dendritic spine maturation in rat hippocampal neurons. *Brain Res.* **1352**, 11–20 (2010).
23. Swiercz, R., Cheng, D., Kim, D. & Bedford, M. T. Ribosomal protein rpS2 is hypomethylated in PRMT3-deficient mice. *J. Biol. Chem.* **282**, 16917–16923 (2007).
24. Swiercz, R., Person, M. D. & Bedford, M. T. Ribosomal protein S2 is a substrate for mammalian PRMT3 (protein arginine methyltransferase 3). *Biochem. J.* **386**, 85–91 (2005).
25. Bachand, F. & Silver, P. A. PRMT3 is a ribosomal protein methyltransferase that affects the cellular levels of ribosomal subunits. *EMBO J.* 2641–2650 (2004).
26. Hsu, S.-H. & Hung, W.-C. Protein arginine methyltransferase 3: A crucial regulator in metabolic reprogramming and gene expression in cancers. *Cancer Lett.* **554**, 216008 (2023).
27. Zhao, S. et al. Arginine methyltransferases PRMT2 and PRMT3 are essential for biosynthesis of plant-polysaccharide-degrading enzymes in *Penicillium oxalicum*. *PLoS Genet.* **19**, e1010867 (2023).
28. Zhi, R. et al. PRMT3 regulates the progression of invasive micropapillary carcinoma of the breast. *Cancer Sci.* **114**, 1912–1928 (2023).
29. Shi, Y. et al. PRMT3-mediated arginine methylation of IGF2BP1 promotes oxaliplatin resistance in liver cancer. *Nat. Commun.* **14**, 1932 (2023).
30. Zhu, J. et al. Asymmetric arginine dimethylation of cytosolic RNA and DNA sensors by PRMT3 attenuates antiviral innate immunity. *Proc. Natl. Acad. Sci. USA* **120**, e2214956120 (2023).
31. Kaniskan, H. Ü. et al. Discovery of potent and selective allosteric inhibitors of protein arginine methyltransferase 3 (PRMT3). *J. Med. Chem.* **61**, 1204–1217 (2018).
32. Kaniskan, H. Ü. et al. A potent, selective and cell-active allosteric inhibitor of protein arginine methyltransferase3 (PRMT3). *Angew. Chem.* **54**, 5166–5170 (2015).
33. Liu, X. et al. In situ capture of chromatin interactions by biotinylated dCas9. *Cell* **170**, 1028–1043 (2017).
34. Tsui, C. et al. dCas9-targeted locus-specific protein isolation method identifies histone gene regulators. *Proc. Natl. Acad. Sci. USA* **115**, E2734–E2741 (2018).
35. He, N. et al. HIV-1 Tat and host AFF4 recruit two transcription elongation factors into a bifunctional complex for coordinated activation of HIV-1 transcription. *Mol. Cell* **38**, 428–438 (2010).
36. Kruk, J. A., Dutta, A., Fu, J., Gilmour, D. S. & Reese, J. C. The multifunctional Ccr4-Not complex directly promotes transcription elongation. *Genes Dev.* **25**, 581–593 (2011).
37. Li, Z., Guo, J., Wu, Y. & Zhou, Q. The BET bromodomain inhibitor JQ1 activates HIV latency through antagonizing Brd4 inhibition of Tat-transactivation. *Nucleic Acids Res.* **41**, 277–287 (2013).
38. Bartholomeeusen, K., Xiang, Y., Fujinaga, K. & Peterlin, B. M. Bromodomain and extra-terminal (BET) bromodomain inhibition activate transcription via transient release of positive transcription elongation factor b (P-TEFb) from 7SK small nuclear ribonucleoprotein. *J. Biol. Chem.* **287**, 36609–36616 (2012).
39. Zhu, J. et al. Reactivation of latent HIV-1 by inhibition of BRD4. *Cell Rep.* **2**, 807–816 (2012).
40. Timmons, A. et al. HSF1 inhibition attenuates HIV-1 latency reversal mediated by several candidate LRAs In Vitro and Ex Vivo. *Proc. Natl. Acad. Sci. USA* **117**, 15763–15771 (2020).
41. Li, X. et al. Infection by diverse HIV-1 subtypes leads to different elevations in HERV-K transcriptional levels in human T cell lines. *Front. Microbiol.* **12**, 662573 (2021).
42. Platt, E. J., Wehrly, K., Kuhmann, S. E., Chesebro, B. & Kabat, D. Effects of CCR5 and CD4 cell surface concentrations on infections by macrophagetropic isolates of human immunodeficiency virus type 1. *J. Virol.* **72**, 2855–2864 (1998).
43. Pearson, R. et al. Epigenetic silencing of human immunodeficiency virus (HIV) transcription by formation of restrictive chromatin structures at the viral long terminal repeat drives the progressive entry of HIV into latency. *J. Virol.* **82**, 12291–12303 (2008).
44. Zhou, Q., Chen, D., Pierstorff, E. & Luo, K. Transcription elongation factor P-TEFb mediates Tat activation of HIV-1 transcription at multiple stages. *EMBO J.* **17**, 3681–3691 (1998).
45. Zhu, Y. et al. Transcription elongation factor P-TEFb is required for HIV-1 tat transactivation in vitro. *Genes Dev.* **11**, 2622–2632 (1997).
46. Bieniasz, P. D., Grdina, T. A., Bogerd, H. P. & Cullen, B. R. Recruitment of cyclin T1/P-TEFb to an HIV type 1 long terminal repeat promoter proximal RNA target is both necessary and sufficient for full activation of transcription. *Proc. Natl. Acad. Sci. USA* **96**, 7791–7796 (1999).
47. Home, P. et al. Altered subcellular localization of transcription factor TEAD4 regulates first mammalian cell lineage commitment. *Proc. Natl. Acad. Sci. USA* **109**, 7362–7367 (2012).
48. Saha, B. et al. TEAD4 ensures postimplantation development by promoting trophoblast self-renewal: An implication in early human pregnancy loss. *Proc. Natl. Acad. Sci. USA* **117**, 17864–17875 (2020).
49. Ruelas, D. S. & Greene, W. C. An integrated overview of HIV-1 latency. *Cell* **155**, 519–529 (2013).
50. Wong, J. K. et al. Recovery of replication-competent HIV despite prolonged suppression of plasma viremia. *Science* **278**, 1291–1295 (1997).
51. Kizito, F. et al. Structural rearrangements in the nucleus localize latent HIV proviruses to a perinucleolar compartment supportive of reactivation. *Proc. Natl. Acad. Sci. USA* **121**, e2202003121 (2024).

52. Li, C., Mori, L. & Valente, S. T. The Block-and-Lock Strategy for Human Immunodeficiency Virus Cure: Lessons Learned from Didehydro-Cortistatin A. *J. Infect. Dis.* **223**, 46–53 (2021).
53. Soliman, S. H. A. et al. Enhancing HIV-1 latency reversal through regulating the elongating RNA Pol II pause-release by a small-molecule disruptor of PAF1C. *Sci. Adv.* **9**, eadf2468 (2023).
54. Horvath, R. M., Dahabieh, M., Malcolm, T. & Sadowski, I. TRIM24 controls induction of latent HIV-1 by stimulating transcriptional elongation. *Commun. Biol.* **6**, 86 (2023).
55. Mittler, G., Butter, F. & Mann, M. A SILAC-based DNA protein interaction screen that identifies candidate binding proteins to functional DNA elements. *Genome Res.* **19**, 284–293 (2009).
56. Singhroy, D. N. et al. Automethylation of protein arginine methyltransferase 6 (PRMT6) regulates its stability and its anti-HIV-1 activity. *Retrovirology* **10**, 73 (2013).
57. Xie, B., Invernizzi, C. F., Richard, S. & Wainberg, M. A. Arginine methylation of the human immunodeficiency virus type 1 Tat protein by PRMT6 negatively affects Tat Interactions with both cyclin T1 and the Tat transactivation region. *J. Virol.* **81**, 4226–4234 (2007).
58. Jin, J. et al. PRMT2 promotes HIV-1 latency by preventing nucleolar exit and phase separation of Tat into the Super Elongation Complex. *Nat. Commun.* **14**, 7274 (2023).
59. Liao, Y. et al. PRMT3 drives glioblastoma progression by enhancing HIF1A and glycolytic metabolism. *Cell Death Dis.* **13**, 943 (2022).
60. Wang, Y. et al. PRMT3-Mediated arginine methylation of METTL14 promotes malignant progression and treatment resistance in endometrial carcinoma. *Adv. Sci.* **10**, e2303812 (2023).
61. Van Den Heuvel, D. et al. A CSB-PAF1C axis restores processive transcription elongation after DNA damage repair. *Nat. Commun.* **12**, 1342 (2021).
62. Li, Z., Deeks, S. G., Ott, M. & Greene, W. C. Comprehensive synergy mapping links a BAF- and NSL-containing “supercomplex” to the transcriptional silencing of HIV-1. *Cell Rep.* **42**, 113055 (2023).
63. Boehm, D., Lam, V., Schnolzer, M. & Ott, M. The lysine methyltransferase SMYD5 amplifies HIV-1 transcription and is post-transcriptionally upregulated by Tat and USP11. *Cell Rep.* **42**, 112234 (2023).
64. Horvath, R. M. & Sadowski, I. CBP/p300 lysine acetyltransferases inhibit HIV-1 expression in latently infected T cells. *iScience* **27**, 111244 (2024).
65. Crespo, R. et al. PCID2 dysregulates transcription and viral RNA processing to promote HIV-1 latency. *iScience* **27**, 109152 (2024).
66. Li, T.-W. et al. KDM5A/B contribute to HIV-1 latent infection and survival of HIV-1 infected cells. *Antiviral Res.* **228**, 105947 (2024).
67. Verma, M. et al. PRMT7 Interacts with ASS1 and Citrullinemia Mutations Disrupt the Interaction. *J. Mol. Biol.* **429**, 2278–2289 (2017).
68. Awasthi, S. et al. DDX49 is an RNA helicase that affects translation by regulating mRNA export and the levels of pre-ribosomal RNA. *Nucleic Acids Res.* **46**, 6304–6317 (2018).
69. Diao, Z. et al. SIRT3 consolidates heterochromatin and counteracts senescence. *Nucleic Acids Res.* **49**, 4203–4219 (2021).
70. Ma, J. et al. iProX: an integrated proteome resource. *Nucleic Acids Res.* **47**, D1211–D1217 (2019).
71. Chen, T. et al. iProX in 2021: connecting proteomics data sharing with big data. *Nucleic Acids Res.* **50**, D1522–D1527 (2022).

Acknowledgements

We thanked Dr. Chiahao Tsua, Clauida Cattoglio, and Carla Inouyea in Robert Tijian lab at the University of California, Berkeley, for valuable advice on conducting the dCas9-targeted chromatin-based purification strategy, and for providing the dCas9 expression plasmid, Prof. Wen Liu from Ximen University for providing the plasmid expressing PRMT3, and Prof. Shan Lu from the University of Massachusetts Medical School for

giving us the MT4 cell line as a gift. This work was supported by funding from the National Natural Science Foundation of China (31900132), the Beijing Natural Science Foundation (7232052), the Chinese Institutes for Medical Research, Beijing (CX23YQ04), and the Capital Medical University and Chinese Institutes for Medical Research, Beijing (KCB2301) to D.Y., Funding for Reform and Development of Beijing Municipal Health Commission (EYGF-WSW-04) to K.Y., funding from Scientific Research Foundation of State Key Laboratory of Vaccines for Infectious Diseases, Xiang An Biomedicine Laboratory (2023XAKJ0102052), National Natural Science Foundation of China (32470588), and the Natural Science Foundation of Xiamen (35022202473020) to Y.X.

Author contributions

D.Y., Q.Z. and K.Y. conceived the project and supervised the study. X.W., Y.X., Lin L., L.J., J.S. and X.L. performed the majority of the biochemical, molecular, and cellular experiments. M.F., Lu L. and W.S. performed flow cytometry analyses. J.H. and D.L. performed the majority of virus infection experiments. R.L., X.G. and C.C. conducted mass spectrometry experiments. Y.G. and Z.X. conducted immunoprecipitation experiments. L.W. and H.C. collected peripheral blood and guided the handling and operation of HIV-1-infected patient cells. Y.H. and F.W. provided helpful discussion throughout the project. D.Y., Q.Z., K.Y. and X.W. drafted the manuscript with the input from all authors. All authors have read and approved the final manuscript.

Competing interests

The authors declare no competing interests.

Additional information

Supplementary information The online version contains supplementary material available at <https://doi.org/10.1038/s41467-025-59578-5>.

Correspondence and requests for materials should be addressed to Kaihu Yao, Qiang Zhou or Dan Yu.

Peer review information *Nature Communications* thanks Matjaz Barboric, Ashutosh Shukla, and Wenyan Zhang for their contribution to the peer review of this work. A peer review file is available.

Reprints and permissions information is available at <http://www.nature.com/reprints>

Publisher's note Springer Nature remains neutral with regard to jurisdictional claims in published maps and institutional affiliations.

Open Access This article is licensed under a Creative Commons Attribution-NonCommercial-NoDerivatives 4.0 International License, which permits any non-commercial use, sharing, distribution and reproduction in any medium or format, as long as you give appropriate credit to the original author(s) and the source, provide a link to the Creative Commons licence, and indicate if you modified the licensed material. You do not have permission under this licence to share adapted material derived from this article or parts of it. The images or other third party material in this article are included in the article's Creative Commons licence, unless indicated otherwise in a credit line to the material. If material is not included in the article's Creative Commons licence and your intended use is not permitted by statutory regulation or exceeds the permitted use, you will need to obtain permission directly from the copyright holder. To view a copy of this licence, visit <http://creativecommons.org/licenses/by-nc-nd/4.0/>.

© The Author(s) 2025